Available online at www.sciencedirect.com
SCIENCE DIRECT®
Journal of Sound and Vibration 271 (2004) 177–207
JOURNAL OF SOUND AND VIBRATION
www.elsevier.com/locate/jsvi

Vibration of plates with sub-structural deduction: a reverse receptance approach

David T. Huang[a,*], Edward C. Ting[b]

[a] *Department of Mechanical Engineering, Lunghwa University of Science and Technology, Taoyuan 333, Taiwan*
[b] *Department of Civil Engineering, Purdue University, West Lafayette, IN 47907, USA*

Received 15 July 2002; accepted 28 February 2003

Abstract

A reverse receptance approach is proposed to find approximate dynamic characteristics of structures with sub-structural deductions. The procedure is a modification of the well-known receptance method commonly used to study vibrations of combined structures. In the paper, vibrations of circular plates with circular central cutouts are studied analytically to illustrate the approach. Numerical results of the frequencies and mode shapes are compared with the available exact solutions and finite element calculations to evaluate the accuracy and the range of applicability. It is found that for a ratio of radii less than 0.3, the errors of approximate solutions are generally less than 1%. The analytical study demonstrates the potential of the reverse receptance concept in the engineering practice of machine design, as a simple numerical or analytical approach to study dynamics of structures with complex geometries.

1. Introduction

In the development of a machine component, it is often necessary to go through an iterative process to define a suitable component geometry that satisfies both the physical need and the performance requirement. This process can be tedious and costly. Thus, finding an expedient way to simplify the process is of great interest to design engineers.

One of the major tasks in this process is to determine the sizes and locations of cutouts or holes to make the components functional and compatible. Engineers need to accurately assess the component performance changes due to these sub-structural deductions and make decisions accordingly. For example, the oscillatory and acoustical properties being altered by a proposed

*Corresponding author. Fax: +886-2-2345-8289.
E-mail address: tyhuang2@ms41.hinet.net (D.T. Huang).

0022-460X/03/$ - see front matter
doi:10.1016/S0022-460X(03)00368-7

deduction can be critical to the component response and to the overall machine performance. A simple approach to assess the effects is to perform complete finite element analyses of the component and perhaps its connecting parts for each proposed deduction. Clearly, such a process can become very cost ineffective and time-consuming. Current practice usually resolves this problem in two ways: The first is to ignore the holes and cutouts, based on the thought that their effects are not significantly large and can be covered by the safety margins. For some components, this seems acceptable. However, for components whose behaviors are sensitive to the boundary conditions and geometry, the effects of deductions cannot be ignored. One example is the vibratory characteristics of a plate or shell structural component. The natural frequencies and associated mode shapes may change drastically due to the existence of cutouts. In these cases, the second way, a sub-structuring deduction procedure may be introduced to modify the stiffness, or the element mesh, around where the holes and cutouts are located. For the rest of the structure, finite element mesh model remains unchanged.

Although various forms of sub-structuring deduction have been extensively used in the general application of finite element and in the design process, comprehensive studies and attempts to standardize the procedure are somewhat lacking. Designers tend to adopt procedures based on intuition and a qualitative assessment of the accuracy. It is then the objective of the present paper to introduce a more rational approach for the sub-structuring deduction. The basic concept proposed in the paper is a reverse receptance. This concept in essence, is a modification of an approximation technique in vibration known as the receptance method. It has been widely used in industry to assess the frequencies and mode shapes of combined structures based on the known characteristics of each component. In the present approach, the deduced sub-structure is treated as a void or negative component, and thus is a reverse receptance.

Although a reverse receptance seems to be similar to the original added receptance, the mathematical and physical natures of the problems are quite different. While the focus of adding a component is to match their essential boundary conditions, it is important that the natural boundary conditions at the free edges are satisfied when a cutout is implemented. While the receptance method has largely been applied to assess the global behaviors of jointed components that are of equal sizes, the sub-structuring deduction is essentially a study of the effect of localization due to components of different sizes. Thus, before a computer algorithm can be developed for general applications, it seems plausible first to assess the applicability and accuracy of the reverse approach.

In this regard, a theoretical analysis of the reverse receptance approach is performed. To keep the analysis simple, vibration of a thin circular annular plate is considered. The plate is treated as the conjunction of two components, namely a circular plate and a circular cutout. By knowing the properties of each circular plate, attempt is to find the approximate frequencies and mode shapes of the annular plate. They are compared with the available analytical solutions. The objective is to answer some important questions. What are the critical parameters when the cutout is introduced? How would the matching of moments, shear forces, in-plane forces, displacements and slopes affect the accuracy? How significant would the errors become as the size of cutout increases? The dynamic analysis includes both the symmetrical and asymmetrical modes.

The published literature related to the dynamic characteristics of a plate with internal cutouts can be found for circular, rectangular or elliptical plates with a single central hole of circular, square or elliptical shape. For an annular plate, Raju [1], Joga-Rao and Pickett [2], Vogel and

Skinner [3] obtained exact solutions of the frequency parameters for the nine possible combinations of boundary conditions, that are simply supported, clamped, and free at the outside and inside boundaries. Joga-Rao and Pickett [2] and Joga-Rao and Vijayakumar [4] studied these cases by using Rayleigh–Ritz method to obtain approximate frequency parameters. For the square and rectangular plates with internal cutouts, Kumai [5] used point-matching method to obtain frequency parameters for a clamped or simply supported square plate with a central circular hole, later, Takahashi [6] applied Rayleigh–Ritz method to solve frequency parameters for a clamped rectangular plate with a central circular hole. Joga-Rao and Pickett [2] applied the Rayleigh–Ritz method to find frequency parameters for a simply supported plate and a free square plate with a central circular hole or a centrally located square hole. Gutierrez et al. [7] investigated transverse vibration of rectangular plates elastically restrained against rotation at the edge with a central free hole. Huang and Wang [8] applied the finite strip method and the receptance method to obtain modal characteristics for an elliptical or a square plate with a central elliptical hole or a symmetrically located slit. Lately, Laura et al. [9] applied the Rayleigh–Ritz method to solve frequency parameters of an elliptical plate with a central circular hole.

A study of the literature shows the difficulties in obtaining analytical solutions of plate vibration. Solutions are available only for plates with a centrally located hole. Rayleigh–Ritz approach is often used to obtain approximate solutions for non-circular shapes. For asymmetrical plates or plates with more than one hole, or with cutouts that are not centrally located, the Rayleigh–Ritz method also becomes difficult to apply. The main problem is to find suitable trial functions that satisfy the free-edge boundary conditions at the cutouts, as well as the plate support conditions. The reverse receptance approach (RRA) treats them as separate structural components, and therefore, seems to have advantages in handling these problems. Hence, the present paper may also be of interest to those who attempt to find analytical solutions of plate dynamics.

In the present work, we first consider a first order RRA, employing either a force connection or a moment connection. Then, we apply a second order RRA, employing both force and moment connections, to calculate the modal characteristics of the annular plate with various inner radii. The accuracy is evaluated by comparing the per cent differences in the natural frequencies obtained using the standard finite element and the RRA. We also examine the adequacy of the RRA in vibration cancellation within the hole area, by comparing the mode shapes.

2. Reverse receptance approach

The receptance method, first proposed by Bishop and Johnson [10], is an analytical approach for dynamic analysis of complex structure. Soedel and Wilken [11,12], Azimi et al. [13–15], S.C. Huang et al. [16–27], Achong [28], Huang and Soedel [29–32] have reported further developments and a variety of applications. They combined properties of different structural forms to obtain the global dynamic characteristics of a connected structure. In the paper by Soedel and Soedel [33], certain structural parts were subtracted from a discretized system, for the first time, by using the receptance approach and employing the point receptances, while in the present work, the line receptances are used for a continuous system.

Briefly, a point receptance is defined as the ratio of a displacement or slope response at a certain point to a harmonic force or moment input at the same or a different point. A line receptance can be defined and treated the same as a point receptance under the condition that the spatial dependencies of the receptance can be eliminated. When a sub-structure is to be removed from a major structure, a reverse receptance is introduced for the sub-structuring deduction by subtracting the line receptances of the sub-structure from those of the major structure along the interfacial lines. For example, an annular plate can be viewed as the case where the smaller circular plate, the sub-structure, is deducted from the larger plate, the major structure, as illustrated in Fig. 1. The circumference of the central hole, which is the periphery of the smaller plate, is the interface between the sub-structure and the major one. In general, there are displacements in three directions and slopes in two directions, together with appropriate line force or line moment connections should be considered at the interface. However, as an approximation, one may impose only the relevant receptances and thus simplify the analysis. For example, if only the axisymmetric modes of lower frequencies of a circular plate are considered, the receptance due to circumferential displacements, in-plane displacements, and circumferential slope changes may be neglected. Only the transverse displacements and the radial slope changes need to be included. The number of loading connections at the interface is then reduced to only two, namely, a line force connection coupled with a line moment connection.

The displacement (or slope) amplitudes X_{Ai} $(i = 1 - 2)$, as functions of harmonic force (or moment) amplitudes F_{Aj} $(j = 1 - 2)$, are

$$\{X_{Ai}\} = [\alpha_{ij}]^{\mathrm{T}}\{F_{Aj}\}, \tag{1}$$

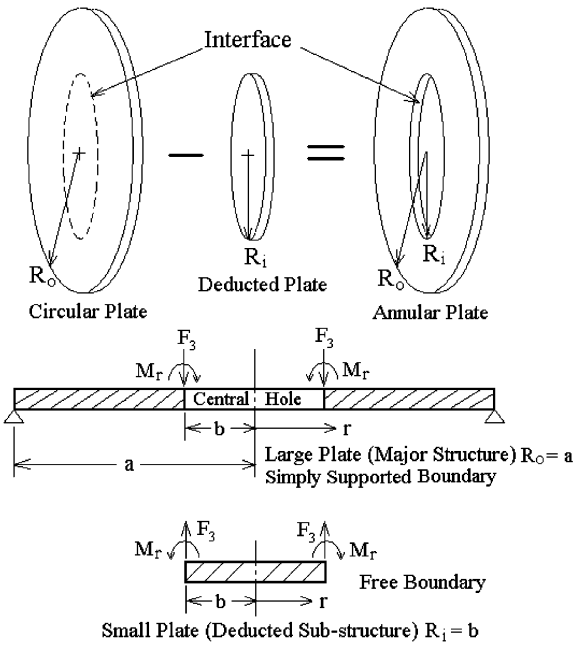

Fig. 1. Illustration of sub-structure deduction concept implemented on an annular plate. Section view shows force and moment connections at the interface between the major structure and the deducted sub-structure.

where the α_{ij} are the receptances of system A, the larger plate shown in Fig. 1. Similarly,

$$\{X_{Bp}\} = [\beta_{pq}]^{\mathrm{T}}\{F_{Bq}\}, \tag{2}$$

where β_{pq} ($p = 1-2$ and $q = 1-2$) are the receptances of system B, the smaller plate to be deducted, as shown in Fig. 1.

When the reverse receptance is applied for deducting a sub-system B from a major system A, with no external forces (or moments) applied to the two systems, it is required that

$$\{F_{Aq}\} = -\{F_{Bq}\} \quad \text{due to the force (or moment) equilibrium, and}$$
$$\{X_{Ap}\} = -\{X_{Bp}\} \quad \text{due to the displacement (or slope) compability.}$$

Combining Eqs. (1) and (2), and applying above equalities gives

$$\begin{bmatrix} \alpha_{11} - \beta_{11} & \alpha_{12} - \beta_{12} \\ \alpha_{21} - \beta_{21} & \alpha_{22} - \beta_{22} \end{bmatrix} \begin{Bmatrix} F_0 \\ M_0 \end{Bmatrix} = 0, \tag{3}$$

where F_0 is the force amplitude and M_0 the moment amplitude. The system frequency equation of the plate-deducted plate (namely, the hole) combination has then the form

$$(\alpha_{11} - \beta_{11})(\alpha_{22} - \beta_{22}) - (\alpha_{12} - \beta_{12})(\alpha_{21} - \beta_{21}) = 0. \tag{4}$$

3. Formulation of receptances

When a circular plate is under free vibration, its equation of motion in transverse direction, which is denoted by subscript 3, can be derived as [34]

$$D\nabla^4 U_3(r,\theta) - \rho h\omega^2 U_3(r,\theta) = 0, \tag{5}$$

where D is the flexural rigidity, ρ the density, h the thickness, ω the forcing frequency and $U_3(r,\theta)$ the modal displacement function of the plate. Upon separating the variables in the modal displacement function and solving the differential equations by taking the boundary conditions into account, the frequency equation can be obtained.

For a clamped circular plate of radius a, the boundary conditions are: for the transverse displacement, $u_3 = 0$, and for the radial slope, $\partial u_3/\partial r = 0$.

The frequency equation is

$$J_n(\lambda a)I_{n+1}(\lambda a) + I_n(\lambda a)J_{n+1}(\lambda a) = 0, \tag{6}$$

where λa are the roots, J_n and I_n the Bessel functions. The modal displacement function is found as

$$U^a_{3mn}(r,\theta) = \left[J_n(\lambda r) - \frac{J_n(\lambda a)}{I_n(\lambda a)} I_n(\lambda r)\right] \cos(n\theta). \tag{7}$$

For a simply supported circular plate of radius a, the boundary conditions are: for the transverse displacement, $u_3 = 0$, and for the moment, $M_{rr} = 0$.

The frequency equation is

$$(1-\nu)[J_n(\lambda a)I_{n+1}(\lambda a) + I_n(\lambda a)J_{n+1}(\lambda a)] = 2(\lambda a)J_n(\lambda a)I_n(\lambda a), \tag{8}$$

where v is the Poisson's ratio. The modal displacement function of a simply supported circular plate has the same form as that of a clamped plate, Eq. (7).

For a free circular plate of radius a, the boundary conditions are: for the moment, $M_{rr} = 0$, and for the shear, $V_{r3} = 0$. The frequency equation can be expressed in the form

$$a_{11}a_{22} - a_{12}a_{21} = 0,$$

where

$$a_{11} = \frac{1}{a^2}\{\lambda a(1-v)J_{n+1}(\lambda a) - [(\lambda a)^2 - (1-v)(n^2-n)]J_n(\lambda a)\}, \tag{9}$$

$$a_{12} = -\frac{1}{a^2}\{\lambda a(1-v)I_{n+1}(\lambda a) - [(\lambda a)^2 + (1-v)(n^2-n)]I_n(\lambda a)\}, \tag{10}$$

$$a_{21} = \frac{1}{a^3}\{\lambda a[(\lambda a)^2 + n^2(1-v)]J_{n+1}(\lambda a) - n[(\lambda a)^2 + (1-v)(n^2-n)]J_n(\lambda a)\}, \tag{11}$$

$$a_{22} = \frac{1}{a^3}\{\lambda a[(\lambda a)^2 - n^2(1-v)]I_{n+1}(\lambda a) + n[(\lambda a)^2 - (1-v)(n^2-n)]I_n(\lambda a)\}. \tag{12}$$

The modal displacement function of a free circular plate of radius a can be expressed as

$$U^a_{3mn} = [J_n(\lambda r) + \Phi_a I_n(\lambda r)]\cos(n\theta), \tag{13}$$

where

$$\Phi_a = -a_{11}/a_{12} = \frac{\lambda a(1-v)J_{n+1}(\lambda a) - [(\lambda a)^2 - (1-v)(n^2-n)]J_n(\lambda a)}{\lambda a(1-v)I_{n+1}(\lambda a) - [(\lambda a)^2 + (1-v)(n^2-n)]I_n(\lambda a)}. \tag{14}$$

The natural frequencies of a circular plate are related to roots of the frequency equation by

$$\omega^a_{mn} = \frac{(\lambda a)^2_{mn}}{a^2}\sqrt{\frac{D}{\rho h}}. \tag{15}$$

The superscript, a, denotes a plate of radius a, while the subscript m is the number of nodal circles and n the number of nodal diameters. The natural frequencies of a plate vary as its boundary conditions change. If the radius of the circular plate is b instead of a, then all a's in Eqs. (6)–(15) should be replaced by b.

3.1. Receptances of an annular plate with the outside simply supported and the inside free

An annular plate can be regarded as a smaller circular plate, the sub-structure, subtracted from a larger plate, the major structure. The transverse displacements and the radial slope of two structural components are the parameters considered at the interface. Fig. 1 shows transverse shear loading coupled with the moment loading at the interface of the major structure, of radius a, and the deducted sub-structure, of radius b.

3.1.1. Receptances of the major structure due to transverse shear force at the interface

For the major structure, the plate of radius a, the transverse shear $F^a_3(r,\theta,t)$ is defined as

$$F^a_3(x,\theta,t) = -F_0\cos(p\theta)\delta(r-r^*)e^{j\omega t}, \tag{16}$$

where F_0 is the amplitude of the shear force, $p=0, 1, 2,\ldots$, $\delta(r-r^*)$ a Dirac-delta function, and r^* the location of the line force. The magnitude of the forcing function, which is located at $r^*=b$ on the simply supported plate of radius a, is

$$\begin{aligned} F_{mn}^{Fa*} &= \frac{1}{\rho h N_{mn}^a}\int_0^a\int_0^{2\pi} U_{3mn}^a F_3^a r\,\mathrm{d}r\,\mathrm{d}\theta \\ &= \frac{-F_0 b}{\rho h N_{mn}^a}\left[J_n(\lambda b)-\frac{J_n(\lambda a)}{I_n(\lambda a)}I_n(\lambda b)\right]\begin{Bmatrix}\pi\\ 2\pi\end{Bmatrix}\begin{matrix}\text{for } n=p\neq 0,\\ \text{for } n=p=0,\end{matrix} \end{aligned} \tag{17}$$

where the superscript a denotes the plate of radius a. The modal mass of the plate of radius a is

$$\begin{aligned} N_{mn}^a &= \int_0^a\int_0^{2\pi}(U_{3mn}^a)^2 r\,\mathrm{d}r\,\mathrm{d}\theta \\ &= \int_0^a\left[J_n(\lambda r)-\frac{J_n(\lambda a)}{I_n(\lambda a)}I_n(\lambda r)\right]^2 r\,\mathrm{d}r\begin{Bmatrix}\pi\\ 2\pi\end{Bmatrix}\begin{matrix}\text{for } n=p\neq 0,\\ \text{for } n=p=0.\end{matrix} \end{aligned} \tag{18}$$

The transverse displacement of the simply supported plate due to shear force has the form

$$u_3^{Fa}(r,\theta,t)=\sum_{m=1}^{\infty}\frac{F_{mn}^{Fa*}U_{3mn}^a(r,\theta)\mathrm{e}^{\mathrm{j}\omega t}}{(\omega_{mn}^a)^2-\omega^2}, \tag{19}$$

where the natural frequency ω_{mn}^a and the modal displacement function $U_{3mn}^a(r,\theta)$ are defined by the Eqs. (15) and (13), where the superscript a denotes the plate of radius a.

(1) The line receptance due to the displacement response of the simply supported plate of radius a to the line force loading at the interface is found to be

$$\alpha_{11}=\frac{u_3^{Fa}(b,\theta,t)}{F_3^a(b,\theta,t)}=\sum_{m=1}^{\infty}\frac{b[J_n(\lambda b)-J_n(\lambda a)I_n(\lambda b)/I_n(\lambda a)]^2}{\rho h N_{mn}^a[(\omega_{mn}^a)^2-\omega^2]}\begin{Bmatrix}\pi\\ 2\pi\end{Bmatrix}\begin{matrix}\text{for } n=p\neq 0,\\ \text{for } n=p=0.\end{matrix} \tag{20}$$

(2) The line receptance due to the slope response of the simply supported plate of radius a to the line force loading at the interface is

$$\alpha_{21}=\frac{-\partial u_3^{Fa}(b,\theta,t)/\partial r}{F_3^a(b,\theta,t)}=\sum_{m=1}^{\infty}\frac{[J_n(\lambda b)-J_n(\lambda a)I_n(\lambda b)/I_n(\lambda a)]\Gamma_s^a}{\rho h N_{mn}^a[(\omega_{mn}^a)^2-\omega^2]}\begin{Bmatrix}\pi\\ 2\pi\end{Bmatrix}\begin{matrix}\text{for } n=p\neq 0,\\ \text{for } n=p=0,\end{matrix} \tag{21}$$

where

$$\Gamma_s^a=-nJ_n(\lambda b)+(\lambda b)J_{n+1}(\lambda b)+\frac{J_n(\lambda a)}{I_n(\lambda a)}[nI_n(\lambda b)+(\lambda b)I_{n+1}(\lambda b)]. \tag{22}$$

The superscript a, and the subscript s, denote the radius a and the simply supported boundary, respectively.

3.1.2. Receptances of the major structure due to a moment loading at the interface

On the plate of radius a, a line moment $M_r^a(r,\theta,t)$ has the form

$$M_r^a(r,\theta,t)=-M_0\cos(p\theta)\delta(r-r^*)\mathrm{e}^{\mathrm{j}\omega t}. \tag{23}$$

The magnitude of the line moment forcing function on the simply supported plate of radius a is

$$F_{mn}^{Ma*} = \frac{1}{\rho h N_{mn}^{a}} \int_0^a \int_0^{2\pi} U_{3mn}^{a} \frac{1}{r} \left[\frac{\partial (M_r^a r)}{\partial r} \right] r \, \mathrm{d}r \, \mathrm{d}\theta$$
$$= \frac{-M_0 \Gamma_s^a}{\rho h N_{mn}^{a}} \left\{ \begin{matrix} \pi \\ 2\pi \end{matrix} \right\} \begin{matrix} \text{for } n = p \neq 0, \\ \text{for } n = p = 0. \end{matrix} \tag{24}$$

The displacement of the simply supported plate due to the moment loading is

$$u_3^{Ma}(r, \theta, t) = \sum_{m=1}^{\infty} \frac{F_{mn}^{Ma*} U_{3mn}^{a}(r, \theta) \mathrm{e}^{\mathrm{j}\omega t}.}{(\omega_{mn}^{a})^2 - \omega^2} \tag{25}$$

(3) The line receptance due to the displacement response of the simply supported plate of radius a to the line moment loading at the interface is

$$\alpha_{12} = \frac{u_3^{Ma}(b, \theta, t)}{M_r^a(b, \theta, t)} = \sum_{m=1}^{\infty} \frac{[J_n(\lambda b) - J_n(\lambda a) I_n(\lambda b)/I_n(\lambda a)] \Gamma_s^a}{\rho h N_{mn}^{a} [(\omega_{mn}^{a})^2 - \omega^2]} \left\{ \begin{matrix} \pi \\ 2\pi \end{matrix} \right\} \begin{matrix} \text{for } n = p \neq 0, \\ \text{for } n = p = 0. \end{matrix} \tag{26}$$

(4) The line receptance due to the slope response of the simply supported plate of radius a to the line moment loading at the interface is

$$\alpha_{22} = \frac{-\partial u_3^{Ma}(b, \theta, t)/\partial r}{M_r^a(b, \theta, t)} = \sum_{m=1}^{\infty} \frac{(\Gamma_s^a)^2/b}{\rho h N_{mn}^{a} [(\omega_{mn}^{a})^2 - \omega^2]} \left\{ \begin{matrix} \pi \\ 2\pi \end{matrix} \right\} \begin{matrix} \text{for } n = p \neq 0, \\ \text{for } n = p = 0. \end{matrix} \tag{27}$$

The receptances α_{12} and α_{21} are equal, which is as expected from the reciprocity theorem.

3.1.3. Receptances of the sub-structure due to a transverse shear force at the interface

On the sub-structure, the unconstrained plate of radius b, the line force has the form

$$F_3^b(x, \theta, t) = F_0 \cos(p\theta) \delta(r - r^*) \mathrm{e}^{\mathrm{j}\omega t}. \tag{28}$$

The magnitude of the forcing function on the free plate of radius b is

$$F_{mn}^{Fb*} = \frac{F_0 b}{\rho h N_{mn}^{b}} [J_n(\lambda b) + \Phi_b I_n(\lambda b)] \left\{ \begin{matrix} \pi \\ 2\pi \end{matrix} \right\} \begin{matrix} \text{for } n = p \neq 0, \\ \text{for } n = p = 0, \end{matrix} \tag{29}$$

where

$$\Phi_b = \frac{\lambda b(1 - \nu) J_{n+1}(\lambda b) - [(\lambda b)^2 - (1 - \nu)(n^2 - n)] J_n(\lambda b)}{\lambda b(1 - \nu) I_{n+1}(\lambda b) - [(\lambda b)^2 + (1 - \nu)(n^2 - n)] I_n(\lambda b)} \tag{30}$$

in which the superscript and the subscript denote the plate of radius b. The modal mass of the plate of radius b is

$$N_{mn}^{b} = \int_0^b [J_n(\lambda r) + \Phi_b I_n(\lambda r)]^2 r \, \mathrm{d}r \left\{ \begin{matrix} \pi \\ 2\pi \end{matrix} \right\} \begin{matrix} \text{for } n = p \neq 0, \\ \text{for } n = p = 0. \end{matrix} \tag{31}$$

Table 1
Comparison of the natural frequencies calculated by FEM and RRA of the first and the second order for a simply supported–free annular plate, where n is the number of nodal diameters; m is the number of nodal circles

n	m	$R_i/R_o = 0.10$				$R_i/R_o = 0.20$				$R_i/R_o = 0.30$				$R_i/R_o = 0.40$			
		RRA F.C.	RRA M.C.	RRA F+M [M/F]	FEM (Hz)	RRA F.C.	RRA M.C.	RRA F+M [M/F]	FEM (Hz)	RRA F.C.	RRA M.C.	RRA F+M [M/F]	FEM (Hz)	RRA F.C.	RRA M.C.	RRA F+M [M/F]	FEM (Hz)
0	0	242	235	236 [485]	240	259	213	231 [−337]	233	280	187	228 [−174]	230	306	162	233 [−101]	235
	1	1523	1374	1453 [−78]	1455	1655	1243	1549 [−17]	1550	1851	1221	1828 [1.1]	1826	3767	3701	2218 [11]	2339
	2	3857	3376	3697 [−20]	3697	4306	3289	4234 [1.0]	4229	7003	6874	4696 [−11]	5290	7376	6294	7025 [−4.9]	7043
1	0	685	685	684 [9.9]	684	690	689	669 [21]	670	707	696	628 [34]	633	743	697	580 [52]	593
	1	2398	2397	2374 [10]	2372	2472	2416	2248 [26]	2247	2642	2553	2251 [382]	2264	2788	2140	2619 [−7.2]	2623
	2	5109	5094	4992 [11]	4975	5394	4804	4879 [172]	4872	5675	4667	5638 [−1.0]	5628	5052	4906	6911 [7.9]	7259
2	0	1253	1254	1253 [−0.61]	1251	1228	1234	1227 [4.9]	1225	1216	1230	1193 [12]	1189	1234	1249	1144 [20]	1143
	1	3418	3424	3418 [1.3]	3410	3381	3410	3320 [8.6]	3318	3512	3473	3207 [20]	3214	3807	3153	3359 [−300]	3354
	2	6536	6556	6529 [2.6]	6508	6626	6627	6317 [12]	6311	7137	6429	6558 [−46]	6564	8723	6178	7732 [2.6]	7882
3	0	1971	1971	1971 [−1.7]	1966	1957	1959	1957 [1.3]	1952	1919	1933	1912 [6]	1910	1885	1920	1826 [11]	1836
	1	4657	4658	4657 [−0.33]	4641	4585	4608	4574 [3.9]	4561	4550	4611	4371 [9.8]	4388	4792	4678	4278 [22]	4352
	2	8293	8298	8293 [0.46]	8251	8159	8232	8051 [5.6]	8025	8485	8340	7873 [18]	7923	9162	7883	8856 [−4]	8859

Note: F.C. and M.C. denote force connection and moment connection, respectively. F + M denotes force plus moment connections. The values in the square brackets are the moment to force amplitude ratios at the fictitious joint of two plates.

The transverse displacement of the free plate of radius b due to the transverse shear force has the form

$$u_3^{Fb}(r,\theta,t)=\sum_{m=1}^{\infty}\frac{F_{mn}^{Fb*}U_{3mn}^{b}(r,\theta)e^{j\omega t}}{(\omega_{mn}^{b})^2-\omega^2}. \tag{32}$$

The natural frequency ω_{mn}^{b} and the modal displacement function $U_{3mn}^{b}(r,\theta)$ have the same form as those given in Eqs. (15) and (13), except all a's in these two equations are replaced by b.

(5) The line receptance due to the displacement response of the free plate of radius b to the line force loading at the interface is

$$\beta_{11}=\frac{u_3^{Fb}(b,\theta,t)}{F_3^{b}(b,\theta,t)}=\sum_{m=1}^{\infty}\frac{b[J_n(\lambda b)+\Phi_b I_n(\lambda b)]^2}{\rho h N_{mn}^{b}[(\omega_{mn}^{b})^2-\omega^2]}\begin{Bmatrix}\pi\\2\pi\end{Bmatrix}\begin{matrix}\text{for } n=p\neq 0,\\ \text{for } n=p=0.\end{matrix} \tag{33}$$

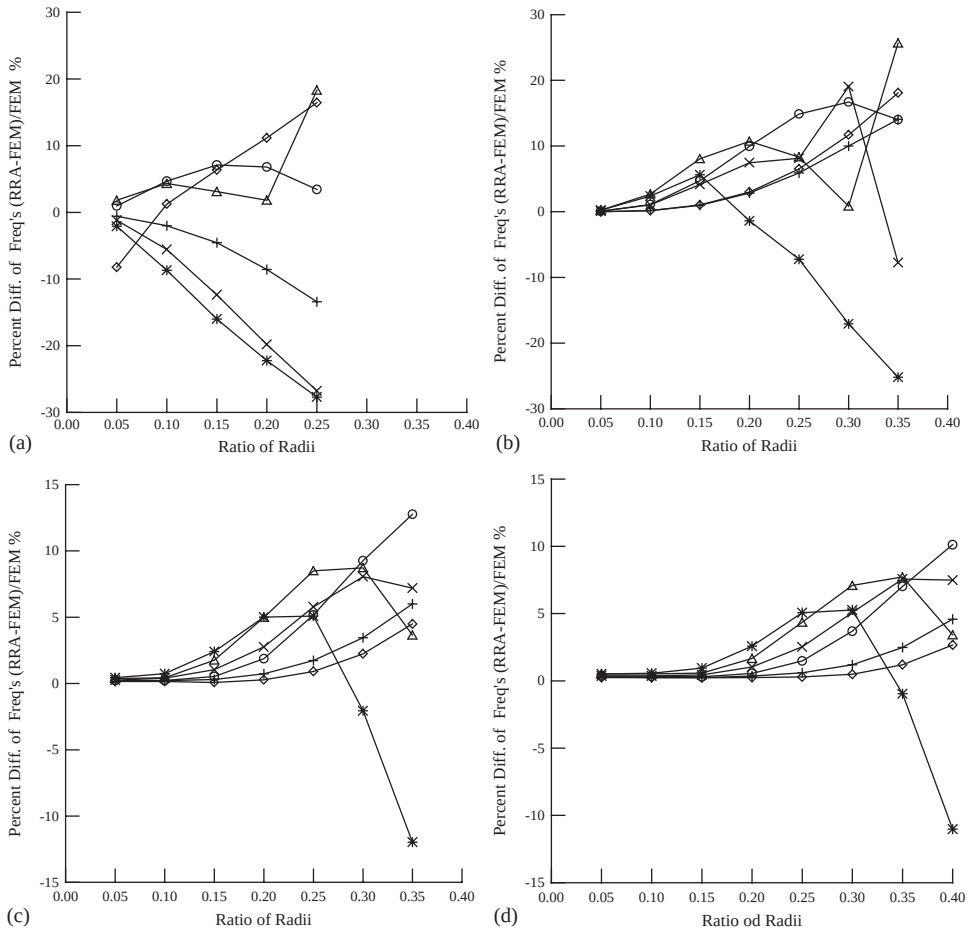

Fig. 2. Per cent difference between natural frequencies obtained by FEM and RRA of the first order (plot (a): modes n0m0 to n0m2; plot (b): modes n1m0 to n1m2; plot (c): modes n2m0 to n2m2; plot (d): modes n3m0 to n3m2. Force connection: (◇) m0, (○) m1, (△) m2; moment connection: (+) m0, (×) m1, (*) m2); and by FEM and RRA of the second order (plot (e): modes n0m0 to n0m2; plot (f): modes n1m0 to n1m2; plot (g): modes n2m0 to n2m2; plot (h): modes n3m0 to n3m2. (◇) m0, (○) m1, (△) m2. The annular plate is simply supported outside and free inside.

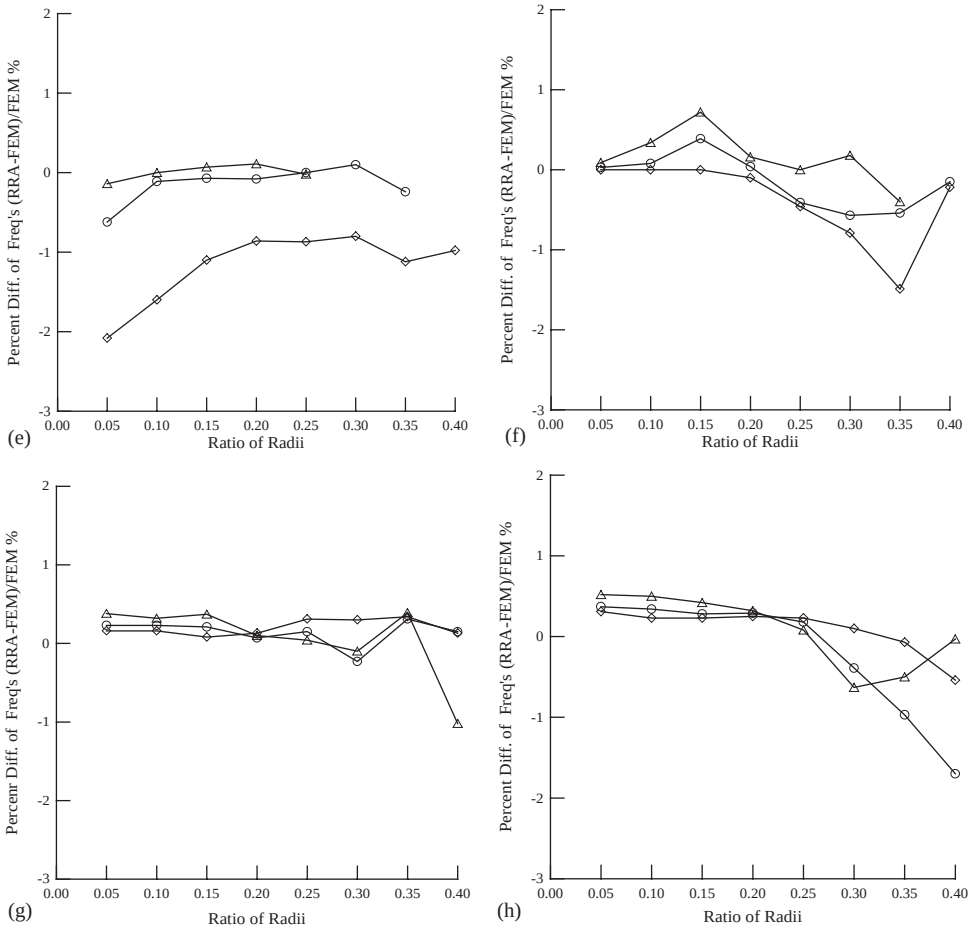

Fig. 2 (*continued*).

Table 2
Comparison of frequency parameters calculated by the second order RRA and the classical method (Vogel/Leissa) for a simply supported–free annular plate

n	m	Frequency parameters (a simply-supported, free annular plate) $\lambda^2 = [\omega(R_o)^2\sqrt{\rho h/D}]$ for values of R_i/R_o of					
		$R_i/R_o = 0.1$			$R_i/R_o = 0.3$		
		RRA (a)	Leissa (b)	$\frac{a-b}{b}\times 100$	RRA (a)	Leissa (b)	$\frac{a-b}{b}\times 100$
0	0	4.74	4.86	−2.5	4.63	4.66	−0.6
	1	29.45	29.4	0.2	37.04	37.0	0.1
	2	74.93	74.8	0.2	95.17	107	−11
1	0	13.86	13.9	−0.3	12.73	12.8	−0.5
	1	48.12	48	0.3	45.61	45.8	−0.4
2	0	25.39	25.4	0	24.17	24.1	0.3
	1	69.26	69.2	0	64.98	65.1	−0.2
3	0	39.93	40.0	−0.2	38.75	38.8	−0.1

(6) The line receptance due to the slope response of the free plate of radius b to the line force loading at the interface is

$$\beta_{21} = \frac{-\partial u_3^{Fb}(b,\theta,t)/\partial r}{F_3^b(b,\theta,t)} = \sum_{m=1}^{\infty} \frac{[J_n(\lambda b) + \Phi_b I_n(\lambda b)]\Gamma_f^b}{\rho h N_{mn}^b[(\omega_{mn}^b)^2 - \omega^2]} \left\{ \begin{array}{c} \pi \\ 2\pi \end{array} \right\} \begin{array}{l} \text{for } n = p \neq 0, \\ \text{for } n = p = 0. \end{array} \tag{34}$$

The function Γ_f^b is defined as

$$\Gamma_f^b = -nJ_n(\lambda b) + (\lambda b)J_{n+1}(\lambda b) - \Phi_b[nI_n(\lambda b) + (\lambda b)I_{n+1}(\lambda b)]. \tag{35}$$

The superscript, b, and the subscript, f, denote the radius b and the free boundary, respectively.

3.1.4. Receptances of the sub-structure due to a moment loading at the interface

On the sub-structure, the free plate of radius b, the line moment is given as

$$M_r^b(r,\theta,t) = M_0 \cos(p\theta)\delta(r - r^*)e^{j\omega t}. \tag{36}$$

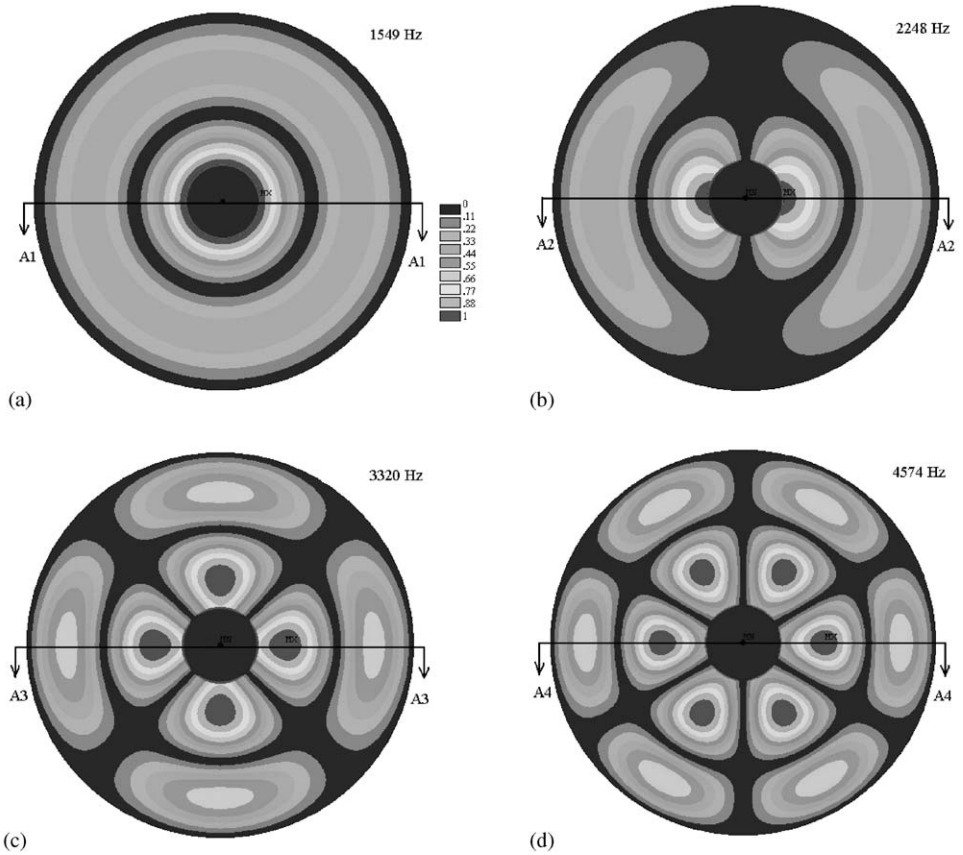

Fig. 3. Modes n0m1, n1m1, n2m1 and n3m1 of a simply supported, free annulus with $R_i/R_o = 0.2$. Plots (a)–(d) show modes obtained by RRA of the second order; plots (e)–(h) show FEM results.

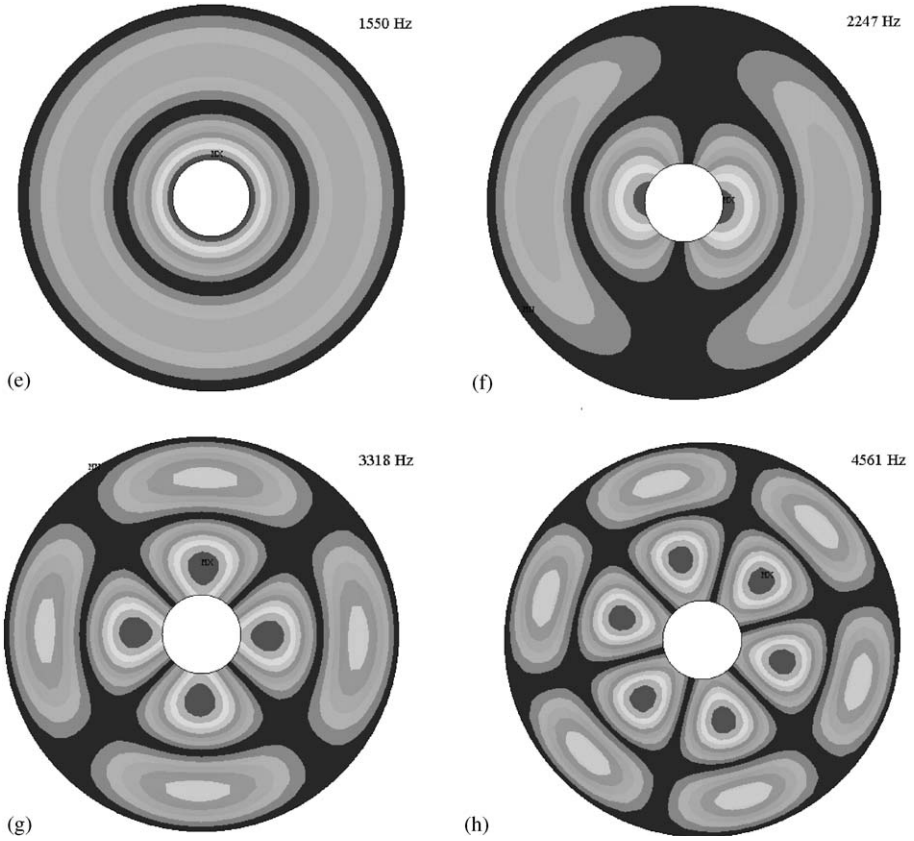

Fig. 3 (*continued*).

The magnitude of the line moment forcing function on the free plate of radius b is

$$F_{mn}^{Mb*} = \frac{M_0 \Gamma_{fe}^b}{\rho h N_{mn}^b} \begin{Bmatrix} \pi \\ 2\pi \end{Bmatrix} \begin{matrix} \text{for } n = p \neq 0, \\ \text{for } n = p = 0. \end{matrix} \tag{37}$$

The transverse displacement of the free plate due to moment loading has the form

$$u_3^{Mb}(r, \theta, t) = \sum_{m=1}^{\infty} \frac{F_{mn}^{Mb*} U_{3mn}^b(r, \theta) e^{j\omega t}}{(\omega_{mn}^b)^2 - \omega^2}. \tag{38}$$

(7) The line receptance due to the displacement response of the free plate of radius b to the line moment loading at the interface is

$$\beta_{12} = \frac{u_3^{Mb}(b, \theta, t)}{M_r^b(b, \theta, t)} = \sum_{m=1}^{\infty} \frac{[J_n(\lambda b) + \Phi_b I_n(\lambda b)] \Gamma_f^b}{\rho h N_{mn}^b [(\omega_{mn}^b)^2 - \omega^2]} \begin{Bmatrix} \pi \\ 2\pi \end{Bmatrix} \begin{matrix} \text{for } n = p \neq 0, \\ \text{for } n = p = 0. \end{matrix} \tag{39}$$

(8) The line receptance due to the slope response of the free plate of radius b to the line moment loading at the interface is

$$\beta_{22} = \frac{-\partial u_3^{Mb}(b,\theta,t)/\partial r}{M_r^b(b,\theta,t)} = \sum_{m=1}^{\infty} \frac{(\Gamma_f^b)^2/b}{\rho h N_{mn}^b[(\omega_{mn}^b)^2 - \omega^2]} \begin{Bmatrix} \pi \\ 2\pi \end{Bmatrix} \begin{matrix} \text{for } n = p \neq 0, \\ \text{for } n = p = 0. \end{matrix} \tag{40}$$

Again as expected, the cross receptances β_{12} and β_{21} are found to be the same due to reciprocity theorem.

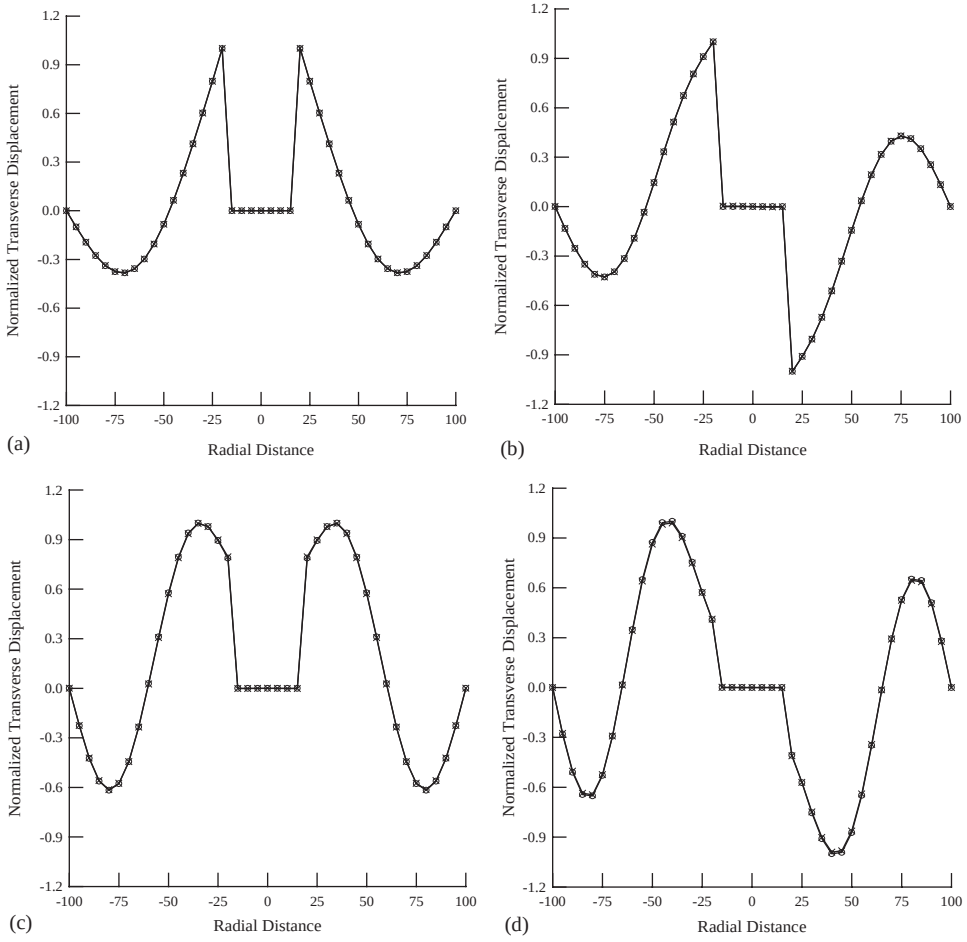

Fig. 4. Displacements on sections (A1–A1 to A4–A4) of modes n0m1 to n3m1 a simply supported, free annular plate with $R_i/R_o = 0.2$. Plots (a)–(d) show results obtained by FEM (○) and RRA of the second order (×); plots (e)–(h) show results obtained by RRAs of the first order (force, △; moment, ○) and the second order (×).

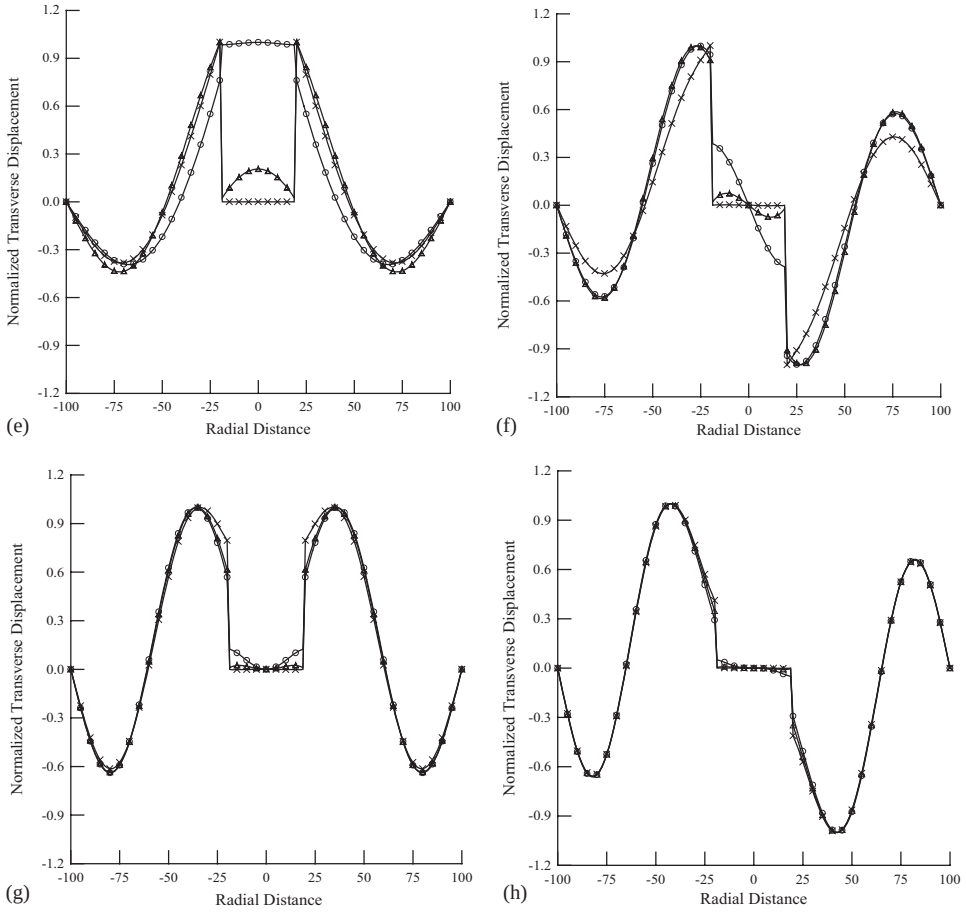

Fig. 4 (*continued*).

3.2. Receptances of an annular plate with outside free and inside clamped

For an annular plate with free boundary at the outside rim and clamped inside, the receptances of the major structure and the deducted sub-structure can be defined in a similar way as given above.

(a) The line receptance due to the displacement response of a free plate of radius a to a line force loading at the interface is

$$\alpha_{11} = \frac{u_3^{Fa}(b,\theta,t)}{F_3^a(b,\theta,t)} = \sum_{m=1}^{\infty} \frac{b[J_n(\lambda b) + \Phi_a I_n(\lambda b)]^2}{\rho h N_{mn}^a[(\omega_{mn}^a)^2 - \omega^2]} \begin{Bmatrix} \pi \\ 2\pi \end{Bmatrix} \begin{matrix} \text{for } n = p \neq 0, \\ \text{for } n = p = 0, \end{matrix} \tag{41}$$

where Φ_a is defined in Eq. (14).

(b) The line receptance due to the slope response of a free plate of radius a to a line force loading at the interface is

$$\alpha_{21} = \frac{-\partial u_3^{Fa}(b,\theta,t)/\partial r}{F_3^a(b,\theta,t)} = \sum_{m=1}^{\infty} \frac{[J_n(\lambda b) + \Phi_a I_n(\lambda b)]\Gamma_f^a}{\rho h N_{mn}^a[(\omega_{mn}^a)^2 - \omega^2]} \begin{Bmatrix} \pi \\ 2\pi \end{Bmatrix} \begin{matrix} \text{for } n = p \neq 0, \\ \text{for } n = p = 0. \end{matrix} \tag{42}$$

The function Γ_f^a is defined as

$$\Gamma_f^a = -nJ_n(\lambda b) + (\lambda b)J_{n+1}(\lambda b) - \Phi_a[nI_n(\lambda b) + (\lambda b)I_{n+1}(\lambda b)]. \tag{43}$$

The line receptance due to the displacement response of a free plate of radius a to a line moment loading at the interface is denoted as α_{12}. The cross receptance α_{12} is equal to α_{21}.

(c) The line receptance due to the slope response of a free plate of radius a to a line moment loading at the interface is

$$\alpha_{22} = \frac{-\partial u_3^{Ma}(b,\theta,t)/\partial r}{M_r^a(b,\theta,t)} = \sum_{m=1}^{\infty} \frac{(\Gamma_f^a)^2/b}{\rho h N_{mn}^a[(\omega_{mn}^a)^2 - \omega^2]} \begin{Bmatrix} \pi \\ 2\pi \end{Bmatrix} \begin{matrix} \text{for } n = p \neq 0, \\ \text{for } n = p = 0. \end{matrix} \tag{44}$$

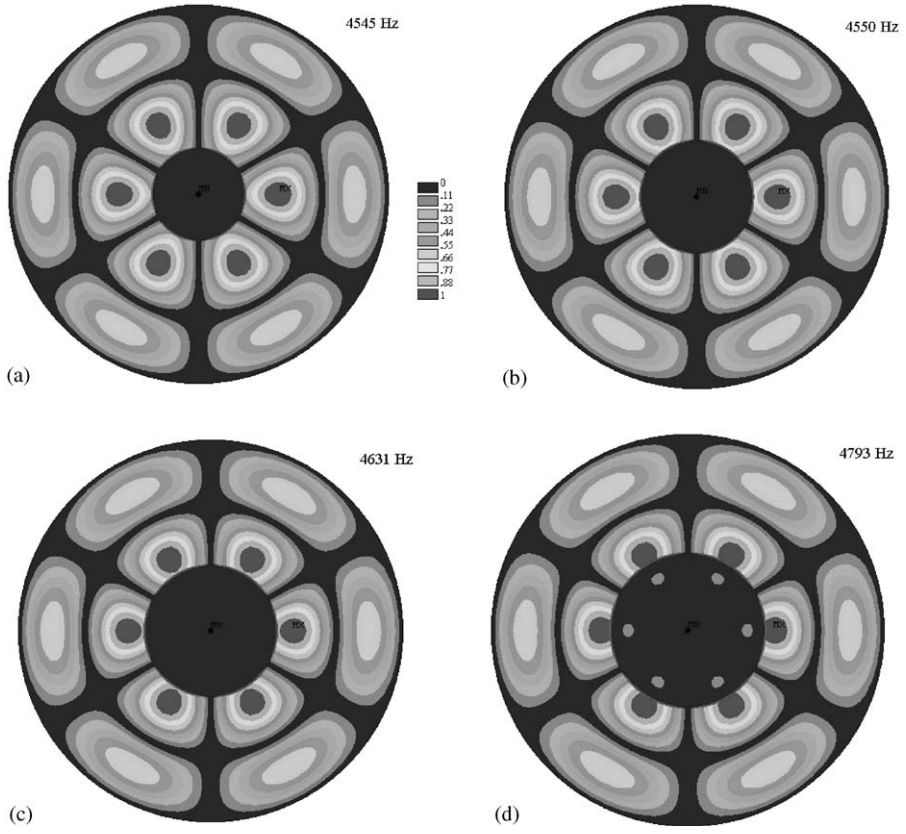

Fig. 5. Variation in shape of mode n3m1 of a simply supported, free annular plate with ratio of radii varies from 0.25 to 0.4. Plots (a)–(d) show results obtained by RRA of the first order using force connection; plots (e)–(h) show that obtained by RRA of the first order using moment connection.

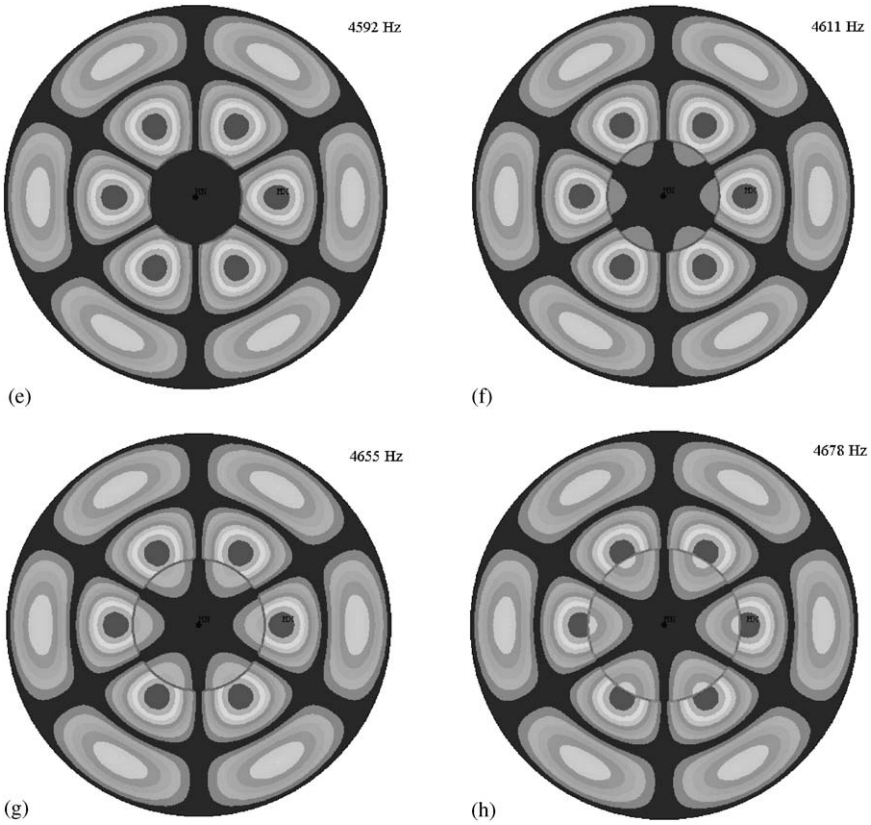

Fig. 5 (*continued*).

The line receptance due to the displacement response of a clamped plate of radius b to a line force loading at the interface is denoted as β_{11}. Since the clamped plate is constrained at $r = b$, the transverse displacement there is zero. So is the receptance β_{12}, which is the line receptance due to the displacement response of the clamped plate of radius b to a line moment loading at the interface. Again, due to the reciprocity theorem, the cross receptance α_{21}, which is the line receptance due to the slope response of the clamped plate of radius b to a line force loading at the interface, is also zero.

(d) The line receptance due to the slope response of the clamped plate of radius b to a line moment loading at the interface is

$$\beta_{22} = \frac{-\partial u_3^{Mb}(b,\theta,t)/\partial r}{M_r^b(b,\theta,t)} = \sum_{m=1}^{\infty} \frac{(\Gamma_c^b)^2/b}{\rho h N_{mn}^b[(\omega_{mn}^b)^2 - \omega^2]} \begin{Bmatrix} \pi \\ 2\pi \end{Bmatrix} \begin{matrix} \text{for } n = p \neq 0, \\ \text{for } n = p = 0. \end{matrix} \tag{45}$$

The function Γ_c^b is defined as

$$\Gamma_c^b = \lambda b[J_{n+1}(\lambda b) + J_n(\lambda b) I_{n+1}(\lambda b)/I_n(\lambda b)]. \tag{46}$$

The superscript, b, and the subscript, c, denote the radius b and the clamped boundary, respectively.

3.3. Receptances of an annular plate with outside and inside free

If an annular plate, as is shown in Fig. 1, is free from constraint on both outside and inside, the receptances of the major structure, α_{11}, α_{21}, α_{12} and α_{22}, can be defined by Eqs. (41)–(44); the receptances of the deducted sub-structure, β_{11}, β_{21}, β_{12} and β_{22}, can be defined by Eqs. (33), (34), (39) and (40).

4. Numerical results

Material properties of steel plates considered in the numerical examples are assumed to be: $E = 20.6\text{e}+4\,\text{N/mm}^2$, $\rho = 7.85\text{e}{-9}\,\text{N s}^2/\text{mm}^4$ and $\upsilon = 0.3$. The dimensions are: outer radius

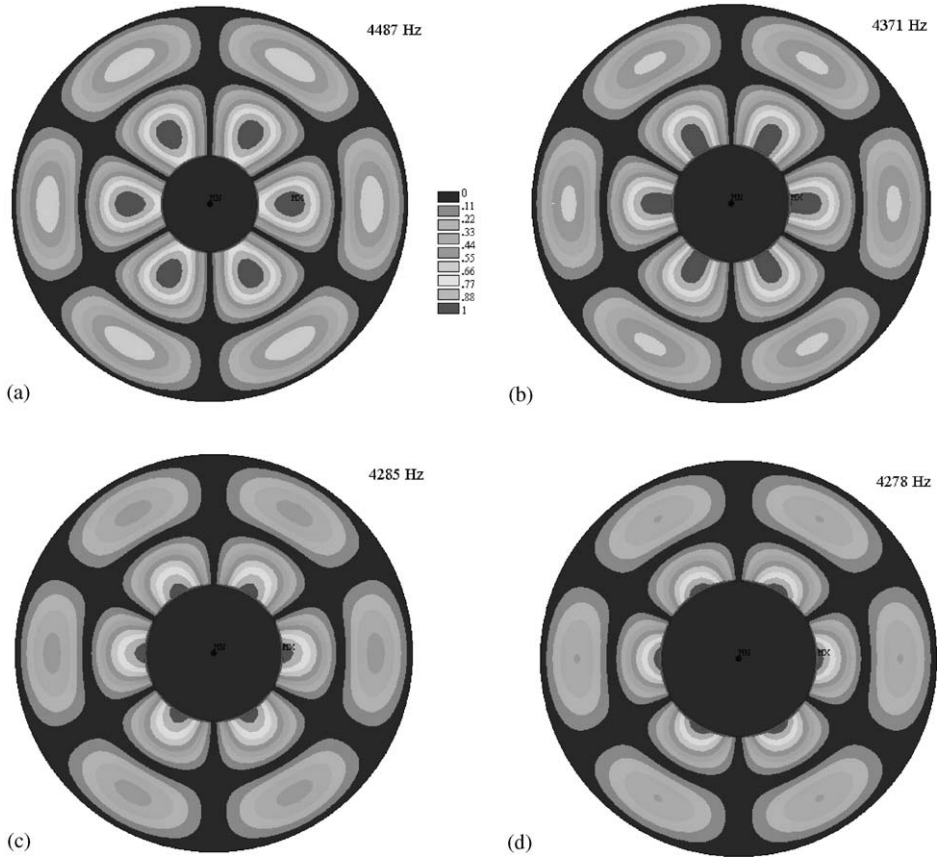

Fig. 6. Variation in shape of mode n3m1 of a simply supported, free annular plate with ratio of radii varies from 0.25 to 0.4. Plots (a)–(d) show results obtained by RRA of the second order (force plus moment connections); plots (e)–(h) show that obtained by FEM.

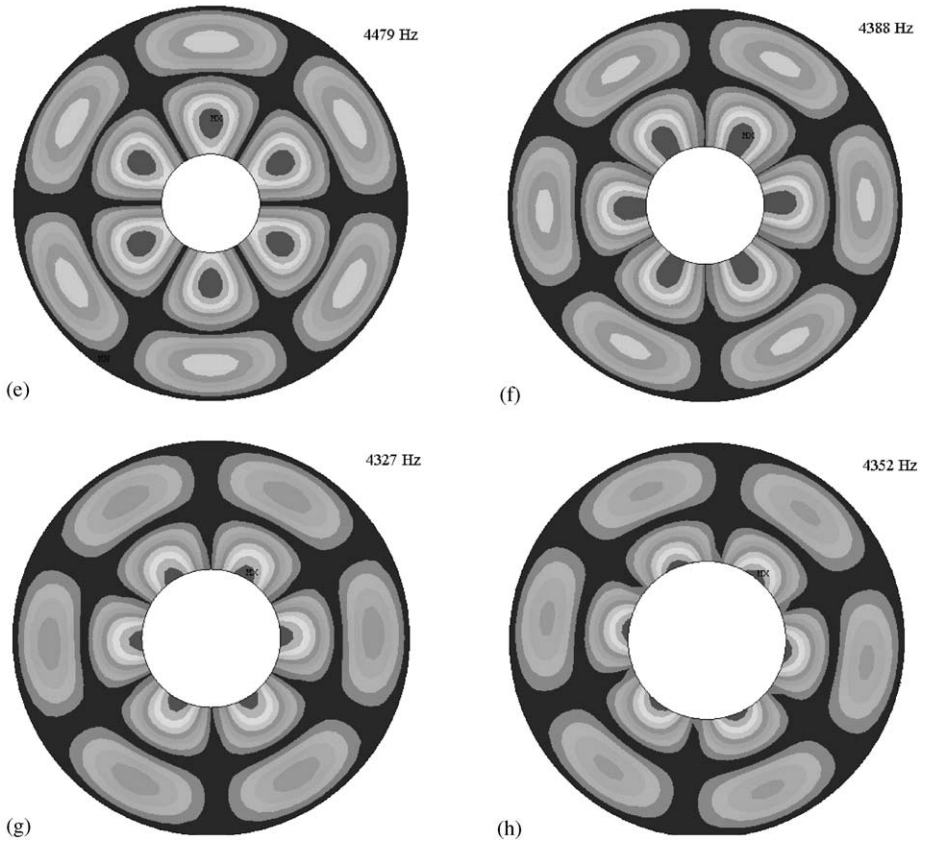

Fig. 6 (*continued*).

$a = 100\,\text{mm}$, thickness $h = 2\,\text{mm}$. The inner radius b is taken as a variable. The modal characteristics of an annular plate with simply supported–free, free–clamped and free–free boundary conditions are calculated.

4.1. An annular plate with outside simply supported and inside free (case 1)

The receptances formulated above are substituted into the system frequency equation, Eq. (4), to numerically evaluate natural frequencies of the combined plate components. Table 1 compares the natural frequencies calculated by FEM and RRA of the first and the second orders of approximation for a simply supported–free annular plate. Finite element results are computed by using a general purpose code ANSYS. In the table, n is the number of nodal diameters, m the number of nodal circles. The frequency results listed in Table 1 are also illustrated in Fig. 2 to show the per cent differences between natural frequencies computed by FEM and RRA. Plots (a)–(d) show the per cent differences for RRA of the first order, considering either a force or a moment connection only. Plots (e)–(h) show the per cent differences for the second order, including both the force and moment connections. From Table 1 and Fig. 2, it can be seen that

assuming a first order RRA, whether it is a force or a moment connection, good accuracy holds when the ratio of radii is small, up to about 0.2–0.25. The errors, which are more sizable at the lower order ($n = 0, 1$) modes, become larger as the ratio of radii increases. The results can be significantly improved by adopting a second order RRA. Good accuracy for the lower order modes can be improved for a ratio of radii up to 0.4.

Table 2 shows comparison of frequency parameters computed by the second order RRA and the exact solutions of the problem (Vogel [3]; Leissa [34]). It is seen that solutions obtained by the second order RRA agree well with the close form solutions.

Substituting each system natural frequency back into the modal displacement equations and calculating displacement responses due to force and moment loadings at each point yields the mode shapes. The modal displacements obtained by RRA are plotted by ANSYS post-processor and compared with ANSYS finite element results. The maximum transverse displacements of all mode shapes are normalized to 1. In Fig. 3, plots (a)–(d) illustrate second order RRA mode

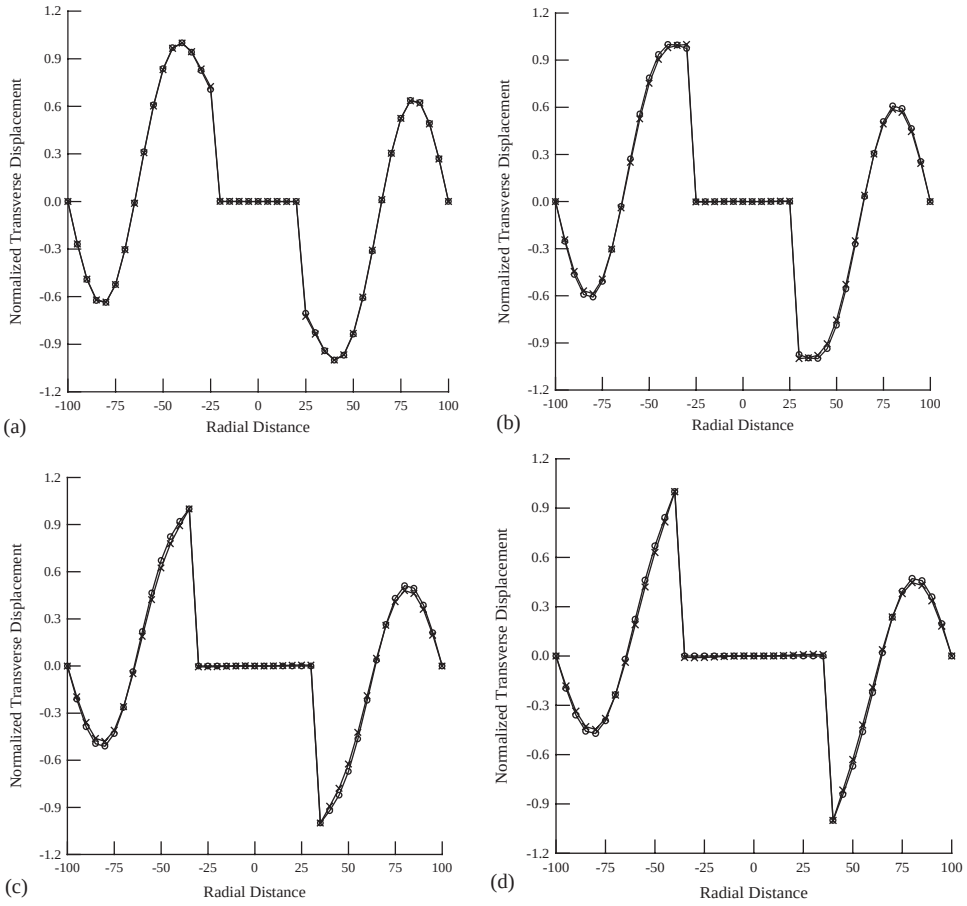

Fig. 7. Displacements on section A4–A4 of mode n3m1 of a simply supported, free annulus with ratio of radii varies from 0.25 to 0.4. Plots (a)–(d) show results obtained by FEM (○) and RRA of the second order (×); plots (e)–(h) show results obtained by RRAs of the first order (force, △; moment, ○) and the second order (×).

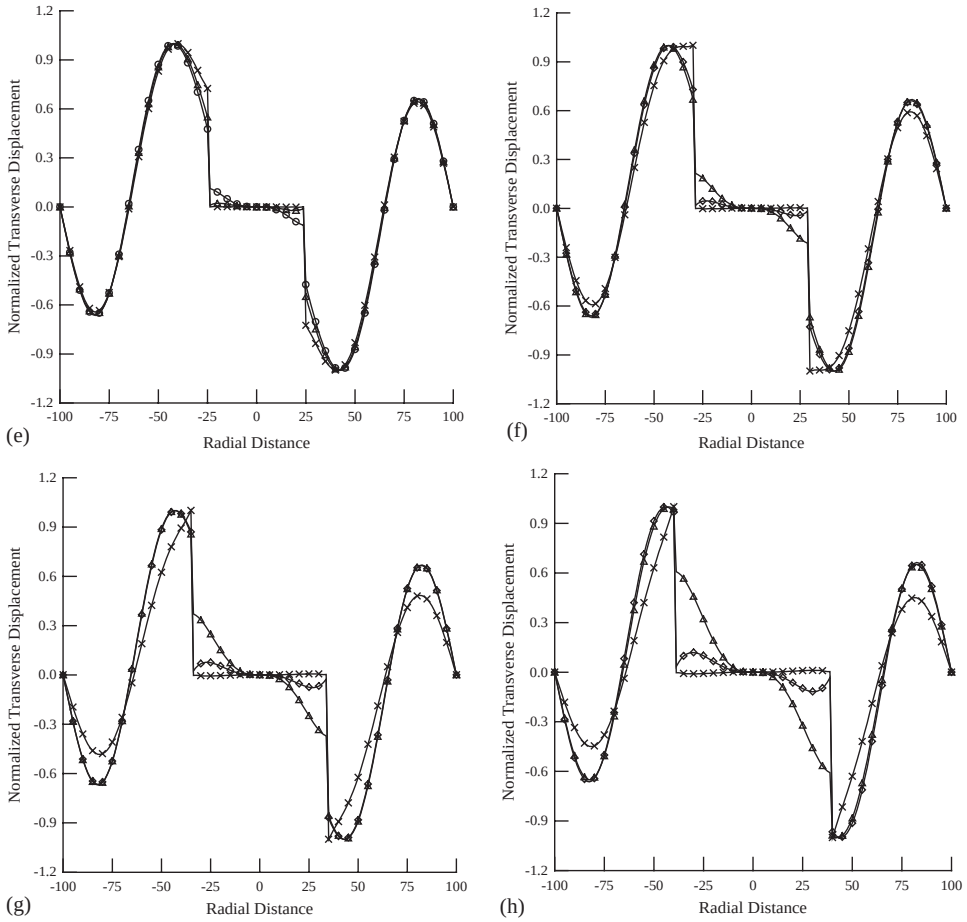

Fig. 7 (*continued*).

shapes n0m1, n1m1, n2m1 and n3m1 of a circular plate with small circular cutouts and simply supported–free boundary conditions. The ratio of radii is 0.2. Plots (e)–(h) illustrate finite element mode shapes of the same problem. Comparing mode shapes displayed side by side in Fig. 3, it is observed that the agreement is quite good.

Fig. 4 shows comparison of normalized transverse displacements of nodes on Sections A1–A1 to A4–A4 (shown also in Fig. 3) of mode shapes n0m1 to n3m1, respectively. It is seen from plots (a)–(d) in Fig. 4, the displacement profiles generated by the second order RRA and FEM agree very well. The transverse vibration of the central area on the circular plate is near zero due to cancellation. In Fig. 4, plots (e)–(h) compare displacement profiles generated by first order RRAs, either a force or a moment connection, and the second order RRA, considering both the force and moment connections. All first order RRAs leads to larger errors. From plots (e)–(g) in Fig. 4, it is found that vibration cancellation cannot be effectively accomplished for nodes inside the cutout area. Errors in the displacements for nodes outside the hole are also seen.

Fig. 5 shows the mode n3m1 of the combined plate, as the ratio of radii increases from 0.25 to 0.40. Plots (a)–(d) display the mode shapes computed by the first order RRA with a force connection only, while plots (e)–(h) are those computed by assuming a moment connection. Using the first order RRA for the mode shapes, the nodal displacements of the plate around the area of cutout cannot be cancelled completely. Residual displacement increases as the ratio of radii increases. They can be observed in plots (d), (f), (g) and (h). From the figures, a moment connection seems less accurate than a force connection.

Fig. 6 plots the same vibration mode of the problem as that in Fig. 5, except that a second order RRA is now employed. Plots (a)–(d) display the mode shapes computed by the second order RRA. Plots (e)–(f) display those computed by using ANSYS finite element code. The

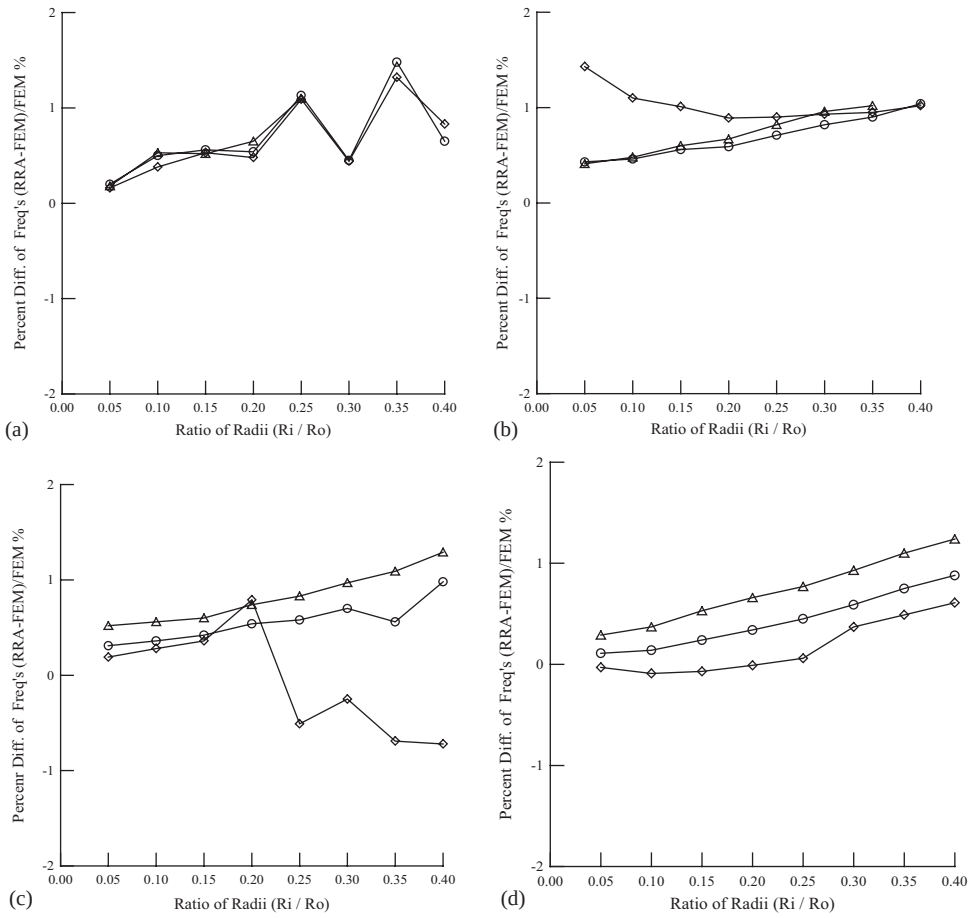

Fig. 8. Per cent difference between natural frequencies obtained by FEM and the sccond order RRA. Plots (a)–(d) show the case of a free, clamped annulus; plots (e)–(h) show that of a free, free annulus. Plot (a): modes n0m0 to n0m2; plot (b): modes n1m0 to n1m2; plots (c) and (g): modes n2m0 to n2m2; plots (d) and (h) modes n3m0 to n3m2; plot (e): modes n0m1 to n0m3; plot (f): modes n1m1 to n1m3. (◇) First frequency, (○) second frequency, (△) third frequency.

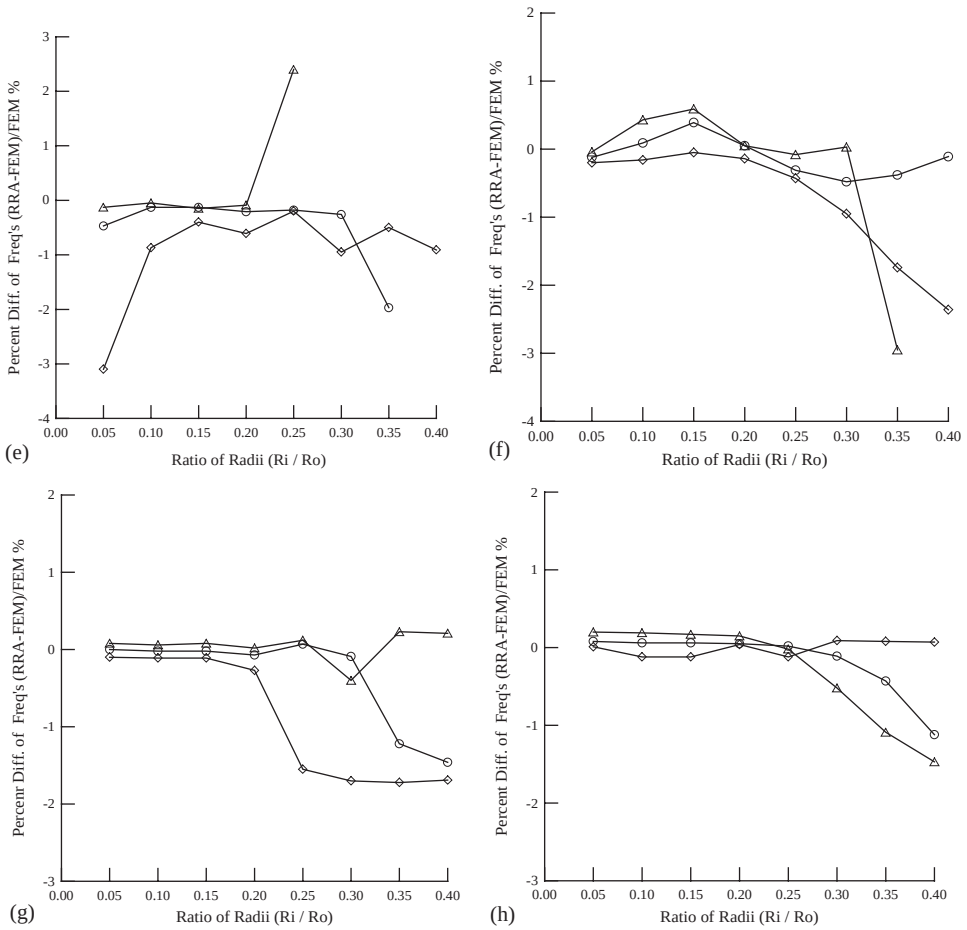

Fig. 8 (*continued*).

displacement cancellation carried out by the second order RRA is more effective for a ratio of radii up to 0.4. The patterns of the modes computed by RRA and FEM are in close agreement.

Plots (a)–(d) of Fig. 7 compare the transverse displacements of nodes on A4–A4 section of mode n3m1 calculated by the second order RRA and FEM for a ratio of radii up to 0.4. Plots (e)–(f) compare the same displacements calculated by RRA of the first and the second order. Errors caused by the insufficient connection conditions at the interface are apparent as the ratio of radii increases.

As a summary, if a force connection only is employed, or a RRA of the first order, the frequencies are overestimated. If a moment connection is employed, the frequencies tend to be underestimated. Errors become noticeable for the higher order ($m \geqq 2$) modes. In general, a force connection seems more accurate than a moment connection. A first order RRA is applicable for lower modes and for smaller radius ratios up to about 0.2. Results are significantly improved if both connections are included. Good accuracy is obtained for radius ratios up to 0.4.

4.2. An annular plate with outside free and inside clamped (case 2)

For the case of an annular plate with outside free and inside clamped, the per cent differences between natural frequencies computed by FEM and the second order RRA are shown in plots (a)–(d) of Fig. 8. It is seen that good accuracy can be obtained for the lower order modes (the number of nodal diameter, n, is up to 3; number of nodal circle, m, is up to 2) with a ratio of radii up to 0.4 or more. The mode shapes, n0m1, n1m1, n2m1 and n3m1, calculated by the second order RRA for a free circular plate with a clamped cutout and a ratio of radii being 0.3 are shown in plots (a)–(d) of Fig. 9. The corresponding mode shapes calculated by FEM for the same annular plate are shown in plots (e)–(h) of Fig. 9. It can be seen that patterns of the mode shapes generated by both approaches are nearly the same. Based on the plots of transverse displacement contours of zero level around the cutout area, it appears that the vibration cancellation is quite effective by using a second order RRA.

In Fig. 11, plots (a)–(d) compare normalized transverse displacements of nodes on sections A1–A1 to A4–A4 of mode shapes n0m1 to n3m1. They correspond to the plots (a)–(d) of Fig. 9.

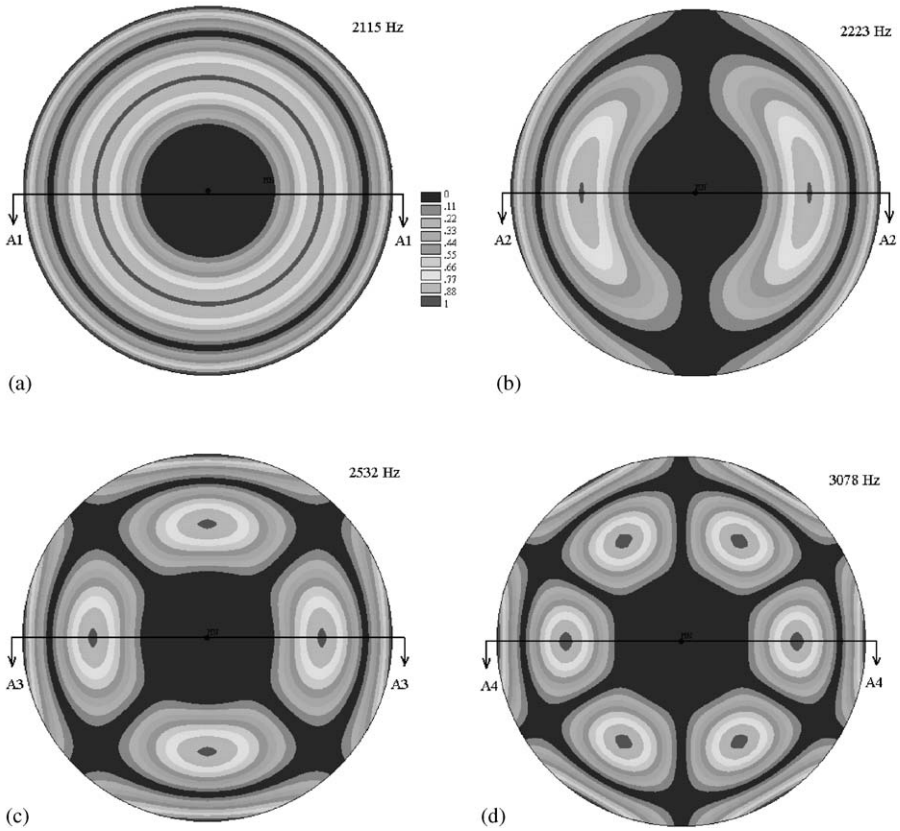

Fig. 9. Modes n0m1, n1m1, n2m1 and n3m1 of a free, clamped annular plate with $R_i/R_o = 0.3$. Plots (a)–(d) show modes obtained by RRA of the second order; plots (e)–(h) show those obtained by FEM.

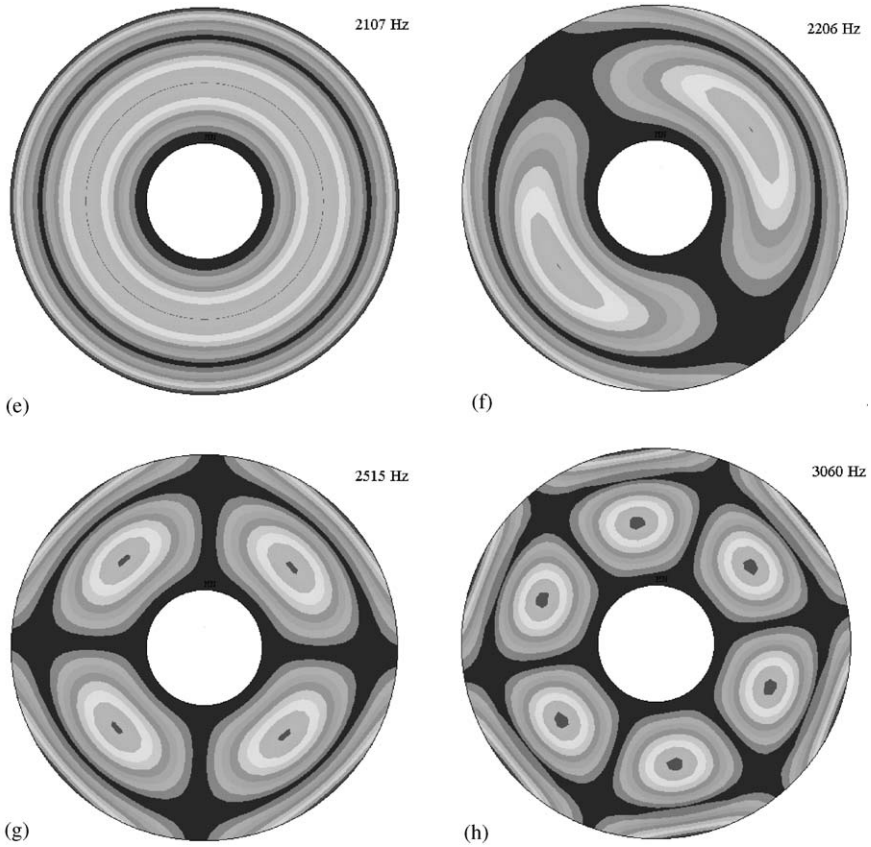

Fig. 9 (*continued*).

Table 3
Comparison of frequency parameters calculated by the second order RRA and the classical method (Vogel/Leissa) for a free–free annular plate

n	m	Frequency parameters (a free, free annular plate) $\lambda^2 = [\omega(R_o)^2\sqrt{\rho h/D}]$ for values of R_i/R_o of					
		$R_i/R_o = 0.1$			$R_i/R_o = 0.3$		
		RRA (a)	Leissa (b)	$\frac{a-b}{b} \times 100$	RRA (a)	Leissa (b)	$\frac{a-b}{b} \times 100$
0	1	8.72	8.77	−0.57	8.29	8.36	−0.84
	2	38.29	38.2	0.24	50.27	50.4	−0.26
1	1	20.40	20.5	−0.49	18.17	18.3	−0.71
	2	59.27	59.0	0.46	58.62	58.8	−0.31
2	0	5.30	5.30	0.00	4.83	4.91	1.63
	1	34.93	34.9	0.09	32.99	33.0	−0.03
3	0	12.44	12.4	0.32	12.29	12.26	0.24
	1	52.97	53.0	−0.06	50.96	51.0	−0.08

The displacement profiles generated by both approaches are about the same except a small difference shown in plot (a). The displacement curves also show zero slopes at the interface.

4.3. An annular plate with outside and inside both free (case 3)

For an annular plate with outside and inside both free, the per cent differences between the natural frequencies computed by FEM and the second order RRA are shown in plots (e)–(h) of Fig. 8. Good accuracy is obtained for the lower order modes with a ratio of radii up to 0.4. Table 3 shows a comparison of frequency parameters computed by the second order RRA and the classical method (Vogel [3]; Leissa [34]) for a free–free annular plate. It is seen that good agreement is obtained. The mode shapes, n0m1, n1m1, n2m1 and n3m1, calculated by the RRA for a free circular plate with a free-edge cutout and a ratio of radii equal to 0.3 are shown in plots (a)–(d) of Fig. 10. The corresponding mode shapes calculated by FEM for the same plate are shown in plots (e)–(h) of Fig. 10. Again, the patterns show good agreement.

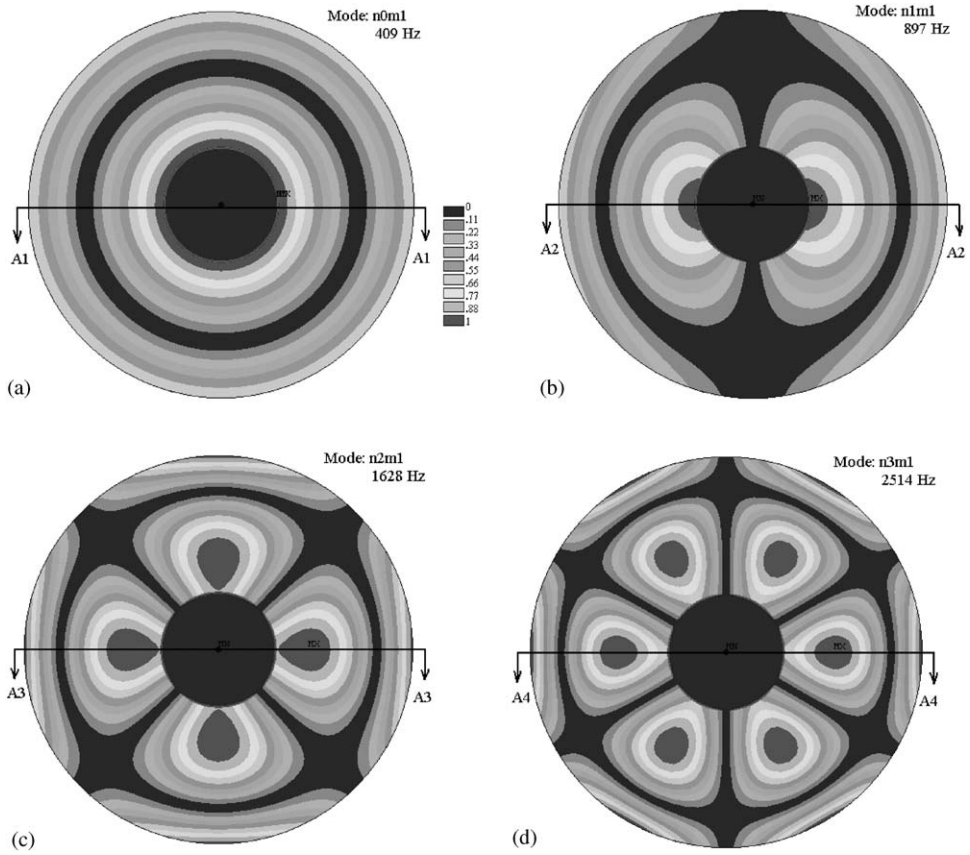

Fig. 10. Modes n0m1, n1m1, n2m1 and n3m1 of a free, free annular plate with $R_i/R_o = 0.3$. Plots (a)–(d) show modes obtained by RRA of the second order; plots (e)–(h) show those obtained by FEM.

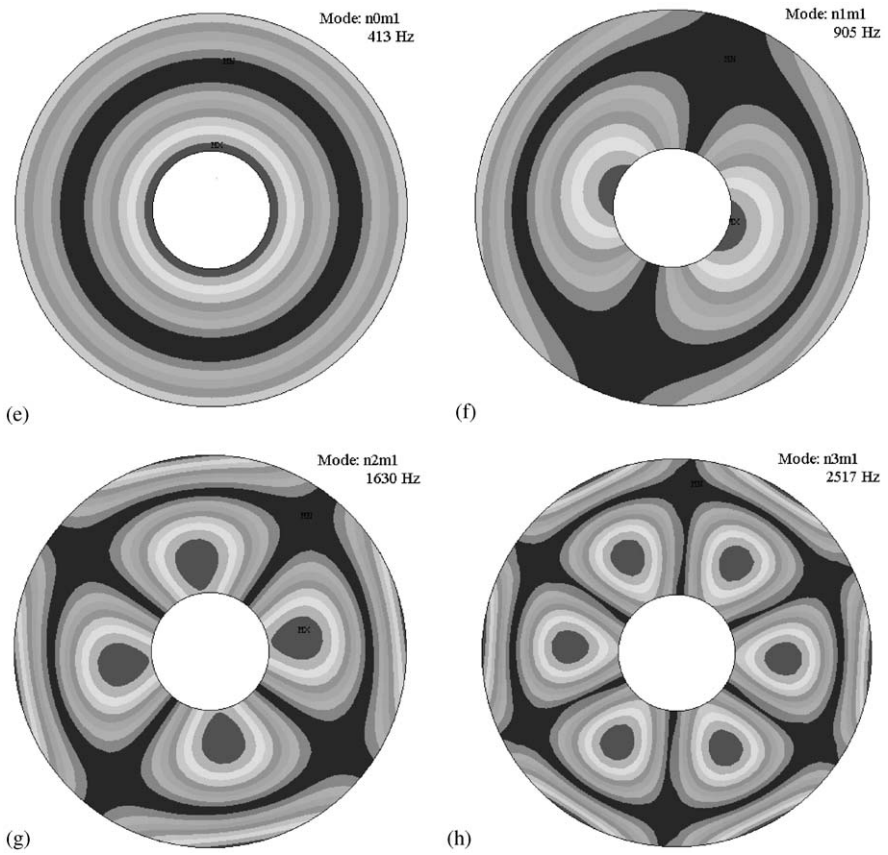

Fig. 10 (*continued*).

In Fig. 11, plots (e)–(h) compare normalized transverse displacements of nodes on sections A1–A1 to A4–A4 of mode shapes n0m1 to n3m1. They correspond to plots (a)–(d) of Fig. 10. Again, the errors are quite small for the frequency range considered.

5. Conclusions

A reverse receptance approach (RRA) is proposed to obtain approximate dynamic characteristics of structures with sub-structuring deductions. The initial motivation for the study is to develop a simple and rational procedure to assess the changes of natural frequencies and mode shapes, due to geometrical alternations in the design of machine components. It is recognized that for engineering practice, this procedure should be numerical in nature, and should consider general three-dimensional structures. However, before embarking on developing large-scale computer algorithms, theoretical studies of the concept for the purpose of evaluating the accuracy and applicability seem warranted. Thus, simple annular plates are chosen for the present study, although the fundamental concept is quite general.

A theoretical study gives vital insights as to how a procedure based on the concept should be carried out. For example, through the accuracy study of annular plates, it is found that the moment and force connections should both be included if the cutouts are relatively large. For smaller holes, a force connection, instead of a moment connection, seems to be an adequate choice. Numerical results also provide verifications of expected results. As the frequency number and the size of cutout increase, the approximation error increases. However, for a central hole as large as 0.4 of the plate diameter, the second order RRA results remain within 1% difference of the exact solution. From the theoretical, as well as the practical point of view, the accuracy and the applicability seem to be satisfactory.

In this study, only lower frequency axisymmetric modes of the plate vibration are evaluated. This is because receptances due to circumferential displacements, in-plane displacements, and circumferential slope changes are neglected. For an annular plate with a small ratio of radii,

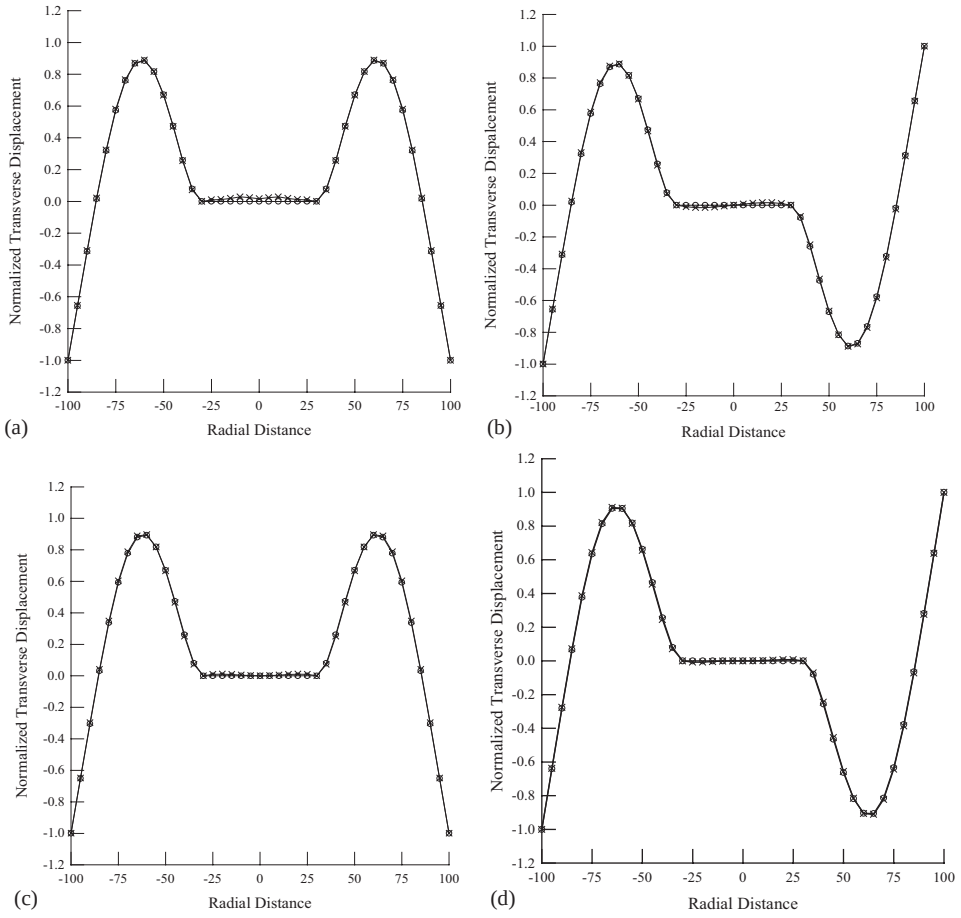

Fig. 11. Displacements on sections (A1–A1 to A4–A4) of modes n0m1 to n3m1 of an annular plate with $R_i/R_o = 0.3$. The results are obtained by FEM (○) and RRA of the second order (×). Plots (a)–(d) show the free, clamped case; plots (e)–(h) show the free, free case.

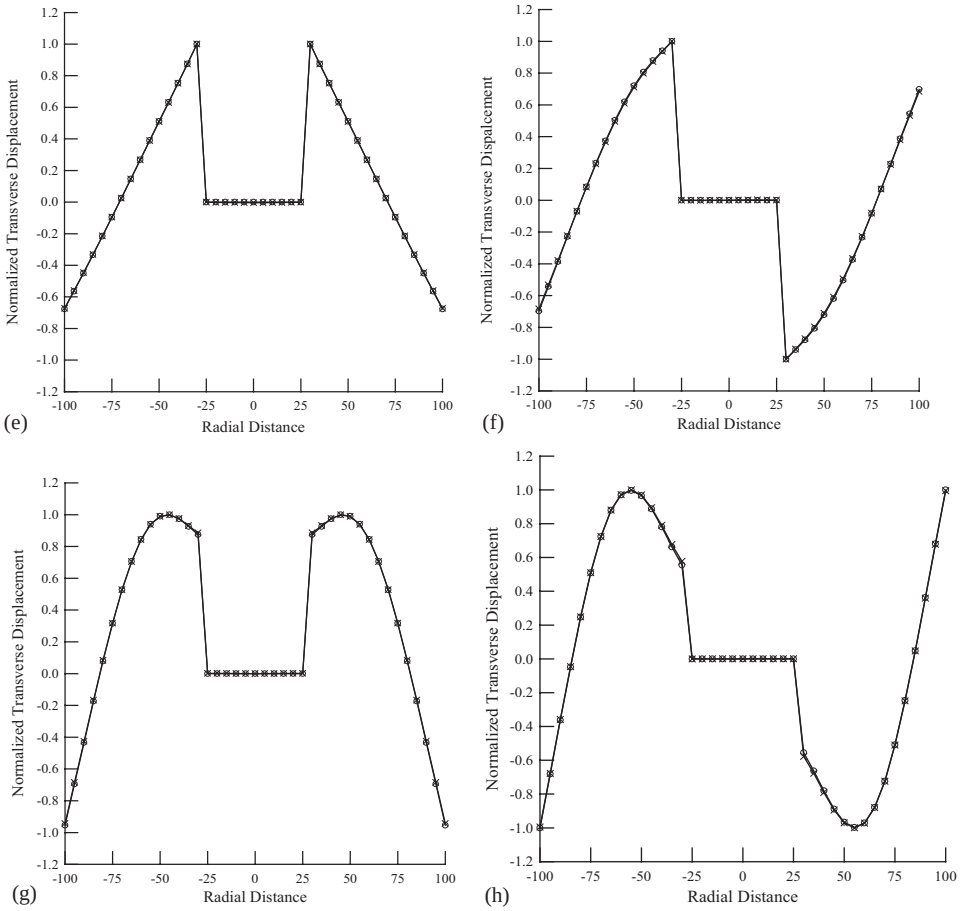

Fig. 11 (*continued*).

transverse modes dominate the vibration in the lower frequency range. It is sufficient only to retain the receptances due to transverse shear forces and bending moments. For higher frequencies and larger cutouts, the in-plane modes of vibration become important. To have better accuracy, the receptances due to in-plane displacements should also be taken into account. The analysis becomes more laborious. However, the concept and solution procedure are similar.

Analytical studies of a bending theory of plates with internal cutouts are in general difficult and complex. The primary difficulty lies in the complexity of boundary conditions. Classical analyses of plate equation are often based on a semi-inverse approach that requires finding trial distribution solutions that satisfy boundary conditions. It is therefore, not hard to find that closed form solutions are only available for limited types of plate geometry. Even by using approximation techniques, such as a Galerkin or Ritz approach, the solution procedures to match all the boundary conditions are still very complex. The proposed RRA essentially treats each set of boundary conditions separately, and then combines the component properties through a set of interaction requirements. Thus, there is considerable flexibility in

handling boundary conditions. Judging from the good accuracy in the numerical results, the approach appears to have the potential as a viable alternative for obtaining analytical solutions.

Acknowledgements

The authors are grateful to the National Science Council of The R.O.C, for the support of this research under grant no. NSC-97-2272-E262-002.

References

[1] P.N. Raju, Vibration of annular plates, Journal of the Aeronautical Society of India 14 (2) (1962) 37–52.
[2] C.V. Joga-Rao, G. Pickett, Vibration of plate of irregular shape and plate with holes, Journal of the Aeronautical Society of India 13 (3) (1961) 83–88.
[3] S.M. Vogel, D.W. Skinner, Natural frequencies of transversely vibrating uniform annular plates, ASME Journal of Applied Mechanics 20 (1965) 926–931.
[4] C.V. Joga-Rao, K. Vijayakumar, On admissible functions for flexural vibration and buckling of annular plate, Journal of the Aeronautical Society of India 15 (1) (1963) 1–5.
[5] T. Kumai, The flexural vibration of a square plate with a central circular hole, Proceedings of the Second Japanese National Congress on Applied Mechanics, 1952, pp. 339–342.
[6] S. Takahashi, Vibration of rectangular plate with central holes, Bulletin of the JSME 1 (4) (1958) 380–385.
[7] R.H. Gutierrez, P.A.A. Laura, J.L. Pombo, Higher frequencies of transverse vibration of rectangular plates elastically restrained against rotation at the edge with a central free hole, Journal of Sound and Vibration 117 (1) (1987) 202–206.
[8] S.C. Huang, J.L. Wang, An approach to the dynamic analysis of confocal elliptic annular plates, Machinery Dynamics and Element Vibrations, 13th ASME Conference on Mechanical Vibration and Noise, DE-Vol.36, 1991, pp. 211–216.
[9] P.A.A. Laura, R.H. Gutierrez, E. Romanelli, Transverse vibrations of a thin elliptical plate with a concentric, circular free edge hole, Journal of Sound and Vibration 146 (4) (2001) 737–740.
[10] R.E.D. Bishop, D.C. Johnson, The Mechanics of Vibration, Cambridge University Press, London, 1960.
[11] I.D. Wilken, W. Soedel, The receptance method applied to ring-stiffened cylindrical shell: analysis of modal characteristics, Journal of Sound and Vibration 44 (1976) 563–576.
[12] I.D. Wilken, W. Soedel, Simplified prediction of the modal characteristics of ring-stiffened cylindrical shell, Journal of Sound and Vibration 44 (1976) 577–589.
[13] S. Azimi, J.F. Hamilton, W. Soedel, The receptance method applied to the free vibration of continuous rectangular plates, Journal of Sound and Vibration 93 (1984) 9–29.
[14] S. Azimi, W. Soedel, J.F. Hamilton, Natural frequencies and modes of cylindrical polygonal ducts using receptance method, Journal of Sound and Vibration 109 (1986) 79–88.
[15] S. Azimi, Free vibration of circular plates with elastic edges supports using the receptance method, Journal of Sound and Vibration 120 (1988) 19–35.
[16] S.C. Huang, W. Soedel, Effects of Coriolis acceleration on the free and forced in-plane vibrations of rotating ring on elastic foundation, Journal of Sound and Vibration 115 (2) (1987) 253–274.
[17] S.C. Huang, W. Soedel, Response of rotating rings to harmonic and periodic loading and comparison with the inverted problem, Journal of Sound and Vibration 118 (2) (1987) 253–270.
[18] S.C. Huang, W. Soedel, Effects of Coriolis acceleration on the forced vibration of rotating cylindrical shells, ASME Journal of Applied Mechanics 55 (1988) 231–233.
[19] S.C. Huang, W. Soedel, On the forced vibration of simply supported rotating cylindrical shells, Journal of the Acoustical Society of America 84 (1) (1988) 275–285.

[20] S.C. Huang, B.S. Hsu, Resonant phenomena of a rotating cylindrical shell subjected to a harmonic moving load, Journal of Sound and Vibration 136 (2) (1990) 215–228.
[21] S.C. Huang, B.S. Hsu, Vibration of spinning ring-stiffened thin cylindrical shells, AIAA Journal 30 (9) (1991) 2291–2298.
[22] S.C. Huang, B.S. Hsu, Receptance theory applied to modal analysis of a spinning disk with interior multi-point supports, ASME Journal of Vibration and Acoustics 114 (1992) 468–476.
[23] S.C. Huang, B.S. Hsu, An approach to the dynamics response of rotating tire–wheel–suspension units, Journal of Sound and Vibration 156 (3) (1992) 505–519.
[24] S.C. Huang, B.S. Hsu, Vibration of spinning annular plate with multi-circular line guides, Journal of Sound and Vibration 164 (3) (1993) 535–547.
[25] S.C. Huang, B.S. Hsu, Modal analysis of a spinning cylindrical shell with interior point or circular line supports, ASME Journal of Vibration and Acoustics 115 (1993) 535–543.
[26] C.K. Su, S.C. Huang, Receptance method to the sensitivity analysis of critical speeds to rotor supports stiffness, ASME Journal of Engineering for Gas Turbines and Power 119 (3) (1996) 736–739.
[27] S.C. Huang, L.H. Chen, Vibration of a spinning cylindrical shell with internal/external ring stiffeners, ASME Journal of Vibration and Acoustics 118 (1996) 227–236.
[28] A. Achong, Vibrations analysis of mass loaded plates and shallow shells by the receptance method with application to steelpan, Journal of Sound and Vibration 191 (2) (1996) 207–217.
[29] D.T. Huang, W. Soedel, Natural frequencies and modes of a circular plate welded to a circular cylindrical shell at arbitrary axial positions, Journal of Sound and Vibration 162 (3) (1993) 403–427.
[30] D.T. Huang, W. Soedel, On the free vibration of multiple plates welded to a cylindrical shell with special attention to mode pairs, Journal of Sound and Vibration 166 (2) (1993) 315–339.
[31] D.T. Huang, W. Soedel, Study of the forced vibration of shell-plate combinations using the receptance method, Journal of Sound and Vibration 166 (2) (1993) 341–369.
[32] D.T. Huang, Influences of small curvatures on the modal characteristics of the joined hermetic shell structures, Journal of Sound and Vibration 238 (1) (2000) 85–111.
[33] D.T. Soedel, W. Soedel, Synthesizing reduced systems by complex receptances, Journal of Sound and Vibration 179 (5) (1994) 855–867.
[34] A.W. Leissa, Vibration of Plates, Office of Technology Utilization, NASA, Washington, DC, 1969.